NASA TECHNICAL NOTE

NASA TN D-6293

NASA TN D-6293

ANALYSIS OF THE THERMAL RESPONSE OF HIGH-DENSITY PHENOLIC-NYLON ON A SPACECRAFT LAUNCHED BY THE PACEMAKER VEHICLE SYSTEM

by William G. Witte

Langley Research Center
Hampton, Va. 23365

NATIONAL AERONAUTICS AND SPACE ADMINISTRATION • WASHINGTON, D. C. • MAY 1971

1. Report No.	2. Government Accession No.	3. Recipient's Catalog No.
NASA TN D-6293		

4. Title and Subtitle	5. Report Date
ANALYSIS OF THE THERMAL RESPONSE OF HIGH-DENSITY PHENOLIC-NYLON ON A SPACECRAFT LAUNCHED BY THE PACEMAKER VEHICLE SYSTEM	May 1971
	6. Performing Organization Code

7. Author(s)	8. Performing Organization Report No.
William G. Witte	L-7230
	10. Work Unit No.
9. Performing Organization Name and Address	709-16-02-01
NASA Langley Research Center Hampton, Va. 23365	11. Contract or Grant No.
	13. Type of Report and Period Covered
12. Sponsoring Agency Name and Address	Technical Note
National Aeronautics and Space Administration Washington, D.C. 20546	14. Sponsoring Agency Code

15. Supplementary Notes

16. Abstract

The thermal response of high-density phenolic-nylon material was determined by a flight test of a recoverable spacecraft. Ablation performance data on the phenolic-nylon were obtained by the use of ablation sensors and thermocouples and by postflight profile-change measurements.

The paper contains a comparison of the flight-test data with predictions based on the Stanford Research Institute correlation. Comparisons of the flight-test data with oxidation-theory predictions are also presented.

The measurements obtained from the ablation sensors and thermocouples used on the spacecraft are discussed.

17. Key Words (Suggested by Author(s))	18. Distribution Statement
Ablation performance High-density phenolic-nylon	Unclassified – Unlimited

19. Security Classif. (of this report)	20. Security Classif. (of this page)	21. No. of Pages	22. Price*
Unclassified	Unclassified	42	$3.00

*For sale by the National Technical Information Service, Springfield, Virginia 22151

ANALYSIS OF THE THERMAL RESPONSE OF HIGH-DENSITY PHENOLIC-NYLON ON A SPACECRAFT LAUNCHED BY THE PACEMAKER VEHICLE SYSTEM

By William G. Witte
Langley Research Center

SUMMARY

The thermal response of high-density phenolic-nylon material was determined by a flight test of a recoverable spacecraft. Ablation performance data on the phenolic-nylon were obtained by the use of ablation sensors and thermocouples and by postflight profile-change measurements.

The paper contains a comparison of the flight-test data with predictions based on the Stanford Research Institute correlation and with oxidation-theory predictions. The measurements obtained from the ablation sensors and thermocouples used on the spacecraft are discussed.

INTRODUCTION

High-density phenolic-nylon material was the standard high-density charring ablator used in correlating the plasma-arc heater facilities in the round-robin study monitored by Stanford Research Institute (SRI) (refs. 1 and 2). It has also been the subject material of numerous oxidation studies (refs. 3 to 8). Because of the interest in this material and the resulting large amount of ground-facility experience with it an investigation was conducted to acquire data at high-velocity flight. A recoverable spacecraft containing the experiments was launched by a Pacemaker vehicle from NASA Wallops Station. A description of the experiment and a presentation of the data obtained from it are contained in reference 9.

The present paper contains a comparison of the flight-test data with surface-recession predictions based on the SRI correlation. The results of the first or low-pressure test phase of that study (ref. 1) showed that mass-loss rates for this material, in these facilities, could be correlated in terms of the stagnation-point heating rate and pressure. The second or high-pressure test phase of that study (ref. 2) showed that this material experienced a rapid increase in ablation above a stagnation pressure of about 2.7 atmospheres.

Comparisons of the flight-test data with oxidation-theory predictions are also given. References 3 to 8 describe oxidation studies of charring ablators using phenolic-nylon. These are stagnation-point studies conducted under conditions of steady-state and quasi-steady-state ablation. Reference 3 considers the effect of pyrolysis gas injection on convective blockage and on the consumption of oxygen in the boundary layer by gas-phase reactions. References 6 to 8 are a series of studies in which various mechanisms, such as chemical reactions, radiative heating and convective blockage, are first isolated and evaluated individually and then considered in relationship to one another. The surface-recession predictions were obtained using Scala's fast and slow oxidation-rate constants (ref. 10).

The measurements obtained from the "state of the art" ablation sensors and thermocouples used on the spacecraft are discussed.

SYMBOLS

Values are given in both SI and U.S. Customary Units. The measurements and calculations were made in U.S. Customary Units.

A	frequency factor, $kg/m^2\text{-}s\text{-}atm^{1/2}$ $(lbm/ft^2\text{-}sec\text{-}atm^{1/2})$
ΔE	activation energy, J/mole (cal/mole)
G	constant in diffusion-limited oxidation equation
H	heat-transfer coefficient, $kg/m^2\text{-}s$ $(lbm/ft^2\text{-}sec)$
K_O	oxygen mass fraction
M_C	molecular weight of carbon
M_O	molecular weight of oxygen
$\dot{m}$	mass-loss rate, $kg/m^2\text{-}s$ $(lbm/ft^2\text{-}sec)$
N	order of reaction
p	pressure, atm
q	heating rate, kW/m^2 $(Btu/ft^2\text{-}sec)$

R	universal gas constant, J/mole-^{o}K (cal/mole-^{o}R)
R_{eff}	effective nose radius, m (ft)
r_n	nose radius, cm (in.)
s	distance along surface measured from stagnation point, cm (in.)
$\dot{s}$	surface recession rate, m/s (ft/sec)
T	absolute temperature, ^{o}K (^{o}R)
t	test time, sec
Δy	distance ablated, m (ft)
ρ	density, kg/m^3 (lbm/ft^3)
ϕ	circumferential location, deg
ψ	convective blocking function

Subscripts:

c	combustion
CR	char removed
cw	cold wall
DL	diffusion limited
e	local (edge of boundary layer)
RL	rate limited
t	total
t,2	total condition behind a normal shock

VM virgin material

w wall

DESCRIPTION OF THE SPACECRAFT AND TEST ENVIRONMENT

The spacecraft (see fig. 1) was a hemispherically blunted cone with a cylindrical afterbody. The thermal protection material on the hemisphere, cone, and forward portion of the cylinder was high-density phenolic-nylon. It was bonded to the primary structure with a layer of elastomeric silicone rubber adhesive approximately 0.0762 to 0.1524 cm (0.030 to 0.060 in.) thick. A detailed description of the spacecraft is given in reference 9. The location of instrumentation on the spacecraft is shown in table I.

The spacecraft was launched by a Pacemaker vehicle. It reached a peak velocity of slightly over 3048 m/s (10 000 ft/sec) at an altitude of 19 812 m (65 000 ft) and coasted to an apogee of 24 384 m (80 000 ft). Telemetered normal and transverse accelerometer data showed no apparent body motions during the data period. The total angle of attack during the data period was less than 3°. The roll rate at third-stage burnout, obtained from a gyro, was 25°/sec.

The computed time histories of cold-wall heating rates, local pressures, and stagnation enthalpy, used in the predictions, are presented in figures 2, 3, and 4. These computations were made for the actual flight trajectory by the methods described in reference 11.

TEST MATERIAL

The composition of the high-density phenolic-nylon used on the spacecraft was 50 percent by weight phenolic and 50 percent by weight ground nylon. The hemisphere-cone section was molded in one piece. The cone-cylinder shoulder section and the cylindrical section were machined from molded billets of the material.

INSTRUMENTATION

The spacecraft was instrumented with spring-wire ablation-rate sensors (ref. 12) and dual ablation-rate sensors. A dual sensor is a spring-wire sensor used in conjunction with a platinum ground wire, with the spring-wire tube and the platinum ground wire forming the elements of a make-wire sensor (ref. 12). The purpose of a spring-wire sensor is to signal when an ablating surface recedes to a particular depth. The spring-wire sensor signals an event when its tube collapses from weakening due to either oxidation or melting. The spring-wire tubes in the nose cap were type 304 stainless steel, with a

melting point of roughly 1700° K (2600° F). The spring-wire tubes in the cylinder were 7075 aluminum, with a melting point of roughly 921° K (1200° F). The purpose of a make-wire sensor is to signal when the electrical conductance at a particular depth in a charring ablator attains a level indicative of a char-pyrolysis zone interface. The make-wire sensors were set to trigger at an electrical resistance of 9800 Ω. This value is considerably lower than the virgin-material resistance. It was chosen with consideration being given to the level of signal noise to which the system was susceptible. It was the lowest value that could be used with an acceptable level of noise. Assuming a density profile through the char similar to that shown in reference 13, this resistance value of 9800 Ω, it is believed, occurs at a location where the density is within a few percent of the virgin-material density.

The spring-wire sensors were installed in arrays of four spring-wire sensors at a location. The dual sensors were installed in arrays of four spring-wire sensors and a platinum ground wire at a location.

Table I presents the locations of the instrumentation. A given circumferential location and surface distance locates the midpoint of the sensor array at that location. For the dual sensors this location corresponds to the location of the platinum ground wire. At the stagnation-point dual sensor, the ground wire is at the theoretical stagnation point and the spring-wire sensors are arranged around it at the corners of a 0.635- by 1.905-cm (0.25- by 0.75-in.) rectangle. In the other dual sensors the spring-wire sensors are arranged 0.635 cm (0.25 in.) from each other in a straight line with the ground wire, with the line perpendicular to a spacecraft longitudinal ray. For the spring-wire sensors the locations given in table I are the midpoints of the arrays. The spring-wire sensors in an array are arranged 0.635 cm (0.25 in.) from each other in a straight line with the midpoint, with the line perpendicular to a spacecraft longitudinal ray. Table II presents the sensing depths of the elements in the sensors. The sensing depths are measured from the outside surface of the spacecraft.

The sensors were seated in holes that had been drilled into the heat shield from the inside of the spacecraft. The holes were nominally 0.051 cm (0.020 in.) in diameter. Most of the holes were "blind" holes, that is, a predetermined thickness of undisturbed heat-shield material remained between the bottom of the hole and the outer surface of the heat shield. Other holes, noted in table II(a), were drilled completely through the heat shield. Previous experience in arc-jet tunnel testing indicated that the type of hole made no difference in the results obtained.

Thermocouples were installed at several locations on the spacecraft (see tables I and III). The thermocouples used in this test were a continuous-reading ribbon type. They were chosen because of their unique ability, when used as surface thermocouples, to furnish continuous readings of an ablating surface. The design of these thermocouples

is such that the broad ribbons forming the leads must be oriented parallel to the direction of heat flow.

TEST RESULTS

Spacecraft Appearance

Figure 5 is a photograph of the recovered spacecraft. The phenolic-nylon ablated almost symmetrically about the spacecraft center line, with slightly greater recession at the 45° station than at the stagnation point. The ground wires and sensor tubes on the hemisphere were exposed and protruded up to 0.7 cm (0.27 in.). (See fig. 6.)

There were large cracks in the phenolic-nylon material (see fig. 6) especially on the cone and cylinder. The bond between the hemisphere and primary structure remained intact, but some separation of the phenolic-nylon from the primary structure occurred on the cone and cylinder. Figure 7 is a photograph of a section taken from the spacecraft in an area where the heat shield had pulled away from and lifted off the primary structure. It is believed that the cracking and separation occurred when the material cooled during the parachute descent of the spacecraft at the conclusion of the flight.

At the separation plane no unusual or excessive ablation occurred although that joint was not bonded.

Overall, the recovered spacecraft was black or dark gray. On the hemisphere and cone, this outer blackened material was crazed (see fig. 6). Streamlines were formed on the cone by alternate stripes of black and variations of gray.

Four distinct zones of surface texture appeared on the spacecraft:

The stagnation point to approximately the 25° station.- The first zone was relatively smooth and evenly ablated although not as smooth to touch as the cone. The outer blackened material was composed of fine-grained particles in a cubic or scalar, rather than a columnar, structure. This structure felt relatively hard as determined by manual prodding with a sharp pointed instrument.

The 25° station to the hemisphere-cone junction.- The second zone was relatively rough and indented. The outer blackened material was composed of fine-grained particles in a columnar structure and was noticeably less hard than that in the first zone.

The cone.- The third zone was the smoothest appearing. The outer blackened material was composed of fine-grained particles in a columnar structure. On the forward portion of the cone, the columnar structure was deeper than that on the hemisphere, but the depth tapered off aftward and

became less deep at the aft end of the cone than on the hemisphere. The outer blackened material seemed to be slightly softer than that of the second zone.

The cylinder.- The fourth zone was relatively smooth with fine streamlines formed by bits of melted material (see fig. 8). The underlying material in this zone seemed to be as hard as virgin material. It was covered with an extremely thin layer, roughly 0.0025 cm (0.001 in.) thick, of soft fine-grained blackened material in addition to the brittle amorphous melted material. This zone did not have the crazed appearance of the other zone. No cubic or columnar structure composed of grainy particles had formed here.

The char structure has been studied in ground tests. Reference 4 presents a description of the internal structure of a phenolic-nylon specimen tested in an arc jet. Four layers are indicated:

(1) A porous black outer layer
(2) A layer having a porous structure in which the nylon has apparently decomposed into gaseous products
(3) A nonporous layer in which the nylon has apparently melted
(4) A layer of virgin material

Reference 4 states that separation frequently occurs between layers (1) and (2), suggesting that the phenolic resin is decomposing at this interface and that the material has little structural strength at this plane. No separation of this kind was evident on the spacecraft. But structural weakness, apparently at this plane, was evident on the previously mentioned second and third zones of the spacecraft. On the first zone structural weakness at this plane occurred to a much lesser degree.

Reference 4 notes that in the arc-jet tests, the crazing (graininess, in their terminology) of the charred material becomes more pronounced as the oxygen content of the test stream decreases and the length of the test increases. Compared with several examples of specimens pictured in reference 4, tested for exposure times of greater than 120 seconds in test streams of various oxygen content, the surface condition of the hemisphere and cone of the recovered spacecraft most closely resembles that of a specimen tested in 5.8-percent oxygen.

Surface-Recession Results

Surface events measured by spring-wire sensors during the flight are presented in table II(a). Twenty-seven of the 40 sensors on the hemisphere were triggered. Thirteen sensors were not triggered. Eight of these were still below the surface after recovery of the spacecraft. However, five of the untriggered spring-wire sensor tubes protruded above the surface at recovery. None of the sensors on the cylinder were triggered.

Postflight measurements of the surface recession are shown in figure 9 at 5° intervals for 12 circumferential locations on the hemisphere. In addition to these longitudinal measurements, measurements were made around the 30°, 40°, 50°, 60°, and 70° stations on the hemisphere. These results are shown in figure 10. These data supported the visual observations that the hemisphere topography of the recovered spacecraft consisted of a relatively smooth evenly ablated area around the stagnation point extending to roughly the 25° station, and aft of that, an area of troughs and ridges. These troughs and ridges extend longitudinally and are most pronounced at roughly the 50° station on the hemisphere.

The cracking and lifting of the heat shield on the cone and cylinder interfered with taking postflight measurements of surface recession at these locations. Some measurements that were obtained indicate surface recession of roughly 0.0254 cm (0.010 in.) on the cone and 0.0025 cm (0.001 in.) on the cylinder.

Char and Pyrolysis-Zone Results

The event times measured by the make-wire function of the dual ablation sensors are presented in table II(b). None of the sensors on the cylinder were triggered.

A visual inspection was made of a section cut from the spacecraft. Measurements were taken along the section from the outer surface to the innermost layer of discolored material, to include the thickness of an outer black porous layer, or char, where one had formed, and the pyrolysis zone. Table IV presents these measurements, the initial depth of the ablator, and average total surface recession for the spacecraft stations.

Thermocouple Measurements

The actual measurements obtained with the surface and in-depth thermocouples located on the cone and cylinder are presented in reference 9. The faired values of these measurements are presented in figure 11.

The thermocouple plug at the 45° station ablated much more than the surrounding material and, therefore, temperature measurements from this location are not presented.

ANALYSIS

Ablation and temperature predictions were made with the aid of the computer program described in reference 14. This program treats ablation as a one-dimensional transient heat-conduction problem with internal decomposition. The surface recession can be specified by several methods. For this analysis surface-recession rates were specified by an empirical method and by an analytical method. The material properties used in making the predictions are listed in table V.

Empirical

In the empirical method surface-recession rates as functions of time were calculated from the SRI correlation (ref. 2) for the stagnation point and the region near the stagnation point (22.5^{o} station). These surface-recession rates were put into the computer program to obtain surface location as a function of time, and surface- and in-depth-temperature histories.

The first step in obtaining surface-recession rate $\dot{s}$ was to compute total mass-loss rate $\dot{m}_t$ as a function of time. This was accomplished with the following formulas from reference 2:

for $p_{t,2} \geqq 2.7$ atm

$$\dot{m}_t = 0.00048(R_{eff})^{-0.32}(q_{cw})^{0.55}(p_{t,2})^{0.88} \tag{1}$$

for $p_{t,2} < 2.7$ atm

$$\dot{m}_t = 0.001(R_{eff})^{-0.32}(q_{cw})^{0.55}(p_{t,2})^{0.13} \tag{2}$$

In the high pressure regime, as shown in reference 2, the char layer is removed as fast as it is formed and $\dot{m}_t$ is essentially equal to the surface-recession rate times the density of the virgin material

$$\dot{m}_t = \dot{s}\rho_{VM} \tag{3}$$

and

$$\dot{s} = \frac{\dot{m}_t}{\rho_{VM}} \tag{4}$$

In the low pressure regime the char-recession rate, from reference 1, is

$$\dot{m}_{CR} = \frac{\rho_{CR}\Delta y}{t} = \rho_{CR}\dot{s} \tag{5}$$

This can be rearranged to obtain

$$\dot{s} = \frac{\dot{m}_{CR}}{\dot{m}_t}\dot{m}_t\frac{1}{\rho_{CR}} \tag{6}$$

A curve of $\dot{m}_{CR}/\dot{m}_t$ versus $p_{t,2}$ was obtained from the data in reference 1. This curve and equations (2) and (6) were then used to compute $\dot{s}$ for the low pressure regime.

The SRI correlation applied to the stagnation point. Therefore, no empirical predictions were made for the 45° and 67.5° stations.

Analytical

The analytical method that was used to specify surface recession was oxidation theory. This method was used to obtain ablation predictions for all of the spacecraft stations. The equations governing the char-layer oxidation are:

In the rate-controlled regime

$$\dot{m}_{c,RL} = A\left(p_e K_{O,e}\right)^{N_c} \exp \frac{\Delta E}{RT_w}$$

where the rate constants used were Scala's fast rate (ref. 10):

Frequency factor, A . . . . . 3.29 Tg/m^2-s-atm$^{1/2}$ (6.729 × 10^8 lbm/ft^2-sec-atm$^{1/2}$)
Activation energy, ΔE . . . . . 184 kJ/mole (44 000 cal/mole)
Order of equation, N_c 0.5

and Scala's slow rate (ref. 10):

Frequency factor, A . . . . . 219 Mg/m^2-s-atm$^{1/2}$ (4.473 × 10^4 lbm/ft^2-sec-atm$^{1/2}$)
Activation energy, ΔE . . . . . 177 kJ/mole (42 300 cal/mole)
Order of equation, N_c 0.5

In the diffusion-controlled regime

$$\dot{m}_{c,DL} = GK_{O,e}\psi H$$

where

$$G = \frac{M_C}{M_O} = 0.75$$

The total char-mass loss was obtained from:

$$\left(\frac{1}{\dot{m}_c}\right)^{1/N_c} = \left(\frac{1}{\dot{m}_{c,RL}}\right)^{1/N_c} + \left(\frac{1}{\dot{m}_{c,DL}}\right)^{1/N_c}$$

The surface-recession rate was obtained from the total char-mass loss rate by

$$\dot{s} = \frac{\dot{m}_c}{\rho_{CR}}$$

This method assumes that the primary reaction product is carbon monoxide and that the pyrolysis products are chemically inert. The only allowed reaction occurring at the char surface is between the char and the oxygen diffusing through the boundary layer.

RESULTS AND DISCUSSION

Sensors

In order for the spring-wire sensors to locate accurately the surface, they require either the attainment of the melting temperature of the spring-wire support tube or an oxidizing atmosphere at a sufficiently high temperature to burn the tube. As mentioned in Surface Recession Results, five of the untriggered spring-wire sensors protruded above the surface at recovery. This may be attributed to the relatively mild conditions during the latter portion of the flight where surface recession occurred at surface temperatures below the melting point of the sensor support tubes. But even at less mild conditions a question can be raised about the performance of these sensors because of the change in environment due to pyrolysis gases. For example, following the initial high-heat pulse on the virgin material, a large efflux of pyrolysis gases may alter the environment by convective blockage or by making it oxygen poor, thus causing a delay in melting or burning of the spring-wire support tubes.

It is believed that the make-wire sensors are good indices of the virgin-material pyrolysis-zone interface. But the depth at which this interface or resistance value occurs varies in time and location on the spacecraft. Under severe conditions where there is negligible char build-up the make-wire sensors for all practical purposes measure surface recession because the virgin-material pyrolysis-zone interface is so close to the surface (ref. 12).

The design of the thermocouples is such that serious errors in the measured temperatures due to conduction of heat along the leads (refs. 15, 16, and 17) can occur. Nevertheless these thermocouples were used because it appeared feasible to conduct a series of ground-facility experiments to obtain a temperature correction. Tests of thermocouples similar to the ones used on the spacecraft were conducted and the temperatures obtained with these thermocouples were compared with temperatures obtained with the photographic pyrometer described in reference 18. Under the quasi-steady-state conditions of these tests the temperatures obtained with the thermocouples lagged the temperatures obtained with the pyrometer. However, these test results are not considered adequate enough to provide a temperature correction.

Predictions

Figure 12 presents the SRI predictions of surface recession compared with data from the spring-wire and make-wire sensors at the stagnation point and at the 22.5° station. The data and predictions for the two locations are similar, except that the spring-wire data seem to indicate the presence of a thick char layer at the stagnation point from 76 to 83 seconds which is greater than the depth of the char and pyrolysis zone measured on the recovered spacecraft. It is believed that the depth of the char layer during the severe heating period (76 to 83 sec) would have been less than that formed during the milder heating period near the conclusion of the flight, which was measured on the recovered spacecraft, because the stagnation-point pressure during the severe heating period was greater than 2.7 atmospheres at which the char is essentially scrubbed away (ref. 2). Therefore the triggering of the two spring-wire sensors is believed to have been delayed. Assuming that the char layer at this time was thin and that the make-wire sensors were essentially measuring surface recession, then the predictions are in good agreement with the first three make-wire data points for the stagnation point and with the first two make-wire data points and the first four spring-wire data points for the 22.5° station. Reference 19 states that when transient predictions are made from steady-state results, in general the calculations overpredict the degradation during decreasing heating. However, figure 12 shows the calculations have underpredicted both the total recession and the last make-wire data point for both the stagnation point and for the 22.5° station. It appears that the last make-wire data point is valid in both cases, compared with the final surface locations.

Figure 13 presents surface-recession predictions based on oxidation theory compared with sensor data for the four stations on the hemisphere. Two sets of predictions were made. One set used the char thermal conductivity of reference 20. The other set used one-third that value, as was done in reference 5, where in steady-state ablation tests no reasonable simultaneous agreement between measured and calculated char-surface temperature, pyrolysis-interface locations, and back-surface temperature rise could be obtained until the value of char conductivity from reference 20 was reduced to one-third. The different values of char conductivity produced small differences in the surface-recession predictions. Slightly greater surface recession was predicted with the lower value of char conductivity than with the higher value. In general, the differences are within the range of accuracy of the sensors.

In all cases (see fig. 13) the slow reaction rate underpredicted the total recession and the fast reaction rate overpredicted the total recession. The fast reaction-rate predictions were in closer agreement with the make-wire data than were the slow reaction rate predictions.

At the stagnation point, where the spring-wire sensors might be expected to be most accurate, because of the clean flow at that location, it appears the spring-wire sensors have been delayed in triggering. At the other stations on the hemisphere, although the spring-wire data are late in comparison to predictions, such as the last point for the 22.5° station, the last point for the 45° station, and most of the points for the 67.5° station, they are within a range of possibility.

The sensors at the 22.5° and 45° stations, in the severe heating period of roughly 70 to 85 seconds, indicated no appreciable char thickness and the predictions are in good agreement with the data. The last spring-wire data points for the 22.5° station and for the 45° station are in agreement with the slow reaction rate predictions. Considering the total recession at these stations these points could be valid.

For the 67.5° station the fast reaction-rate prediction is in good agreement with the make-wire data but overpredicts surface recession compared with most of the spring-wire data. Due to the thick char and pyrolysis zone that formed at this station, and to the difference between the maximum and minimum total recession at this station, all of the spring-wire data here are within the range of possibility.

Figure 11 presents a comparison of measured temperature-time histories and computed values for the cone and cylinder. In all cases the measured temperatures are considerably less than the computed values. It is believed that while downstream cooling by the pyrolysis gases contributes partially to these differences, the conduction of heat along the thermocouple leads is the major contributor.

CONCLUDING REMARKS

Ablation sensors and thermocouples were used to measure the thermal response of phenolic-nylon material at high-velocity flight and the flight data were compared with predictions of surface recession based on the Stanford Research Institute (SRI) correlation and with oxidation-theory predictions.

Under some ablation conditions the spring-wire sensors failed to measure surface location. They indicated the presence of a thick char layer at the stagnation point during the peak pressure and heating period which would, in fact, have been scrubbed away at the pressure levels reached in this region at this time. Therefore the stagnation-point sensors experienced a delay in triggering. Also, some of the sensors on the spacecraft hemisphere became exposed during the mild ablation conditions toward the end of the flight but were not triggered.

The spring-wire sensor data were in good agreement with the oxidation-theory surface-recession predictions for the 22.5° and 45° stations but were late for the stagnation point and the 67.5° station.

The make-wire sensors probably measure accurately the attainment of the electrical conductance which they are set to measure but the in-depth location of such a level of conductance is not precisely determined. Predictions of surface recession based on the SRI correlation coincided with make-wire data of the stagnation point and the 25^{o} station during the peak pressure and heating period when sensors were essentially measuring surface recession because of the thin char layer at this time. However, during the latter portion of the flight the data indicate greater surface recession than the SRI prediction.

At all stations the total recession is within the limits of oxidation-theory predictions made by using both slow and fast reaction rates.

The ribbon-type thermocouples used on the spacecraft have temperature measurements with serious errors which are apparently due to conduction of heat along the ribbons.

Langley Research Center,
National Aeronautics and Space Administration,
Hampton, Va., April 7, 1971.

REFERENCES

1. Hiester, Nevin K.; and Clark, Carroll F.: Feasibility of Standard Evaluation Procedures for Ablating Materials. NASA CR-379, 1966.

2. Hiester, Nevin K.; and Clark, Carroll F.: Comparative Evaluation of Ablating Materials in Arc Plasma Jets. NASA CR-1207, 1968.

3. Walberg, Gerald D.: Analytical Study of Diffusion-Controlled Char Oxidation and Its Effect on Steady-State Ablation of Plastic Materials. NASA TR R-242, 1966.

4. Dow, Marvin B.; and Swann, Robert T.: Determination of Effects of Oxidation on Performance of Charring Ablators. NASA TR R-196, 1964.

5. McLain, Allen G.; Sutton, Kenneth; and Walberg, Gerald D.: Experimental and Theoretical Investigation of the Ablative Performance of Five Phenolic-Nylon-Based Materials. NASA TN D-4374, 1968.

6. Lundell, John H.; Wakefield, Roy M.; and Jones, Jerold W.: Experimental Investigation of a Charring Ablative Material Exposed to Combined Convective and Radiative Heating. AIAA J., vol. 3, no. 11, Nov. 1965, pp. 2087-2095.

7. Lundell, John H.; Dickey, Robert R.; and Jones, Jerold W.: Performance of Charring Ablative Materials in the Diffusion Controlled Surface Combustion Regime. AIAA Paper No. 67-328, Apr. 1967.

8. Wakefield, Roy M.; Lundell, John H.; and Dickey, Robert R.: The Effects of Oxygen Depletion in Gas-Phase Chemical Reactions on the Surface Recession of Charring Ablators. AIAA Paper No. 68-302, Apr. 1968.

9. Witte, William G.: Flight Test of High-Density Phenolic-Nylon on a Spacecraft Launched by the Pacemaker Vehicle System. NASA TM X-1910, 1969.

10. Scala, Sinclaire M.: The Ablation of Graphite in Dissociated Air. Pt. I: Theory. Tech. Inform. Ser. No. R62SD72, Missile Space Div., Gen. Elec. Co., Sept. 1962.

11. Graves, Randolph A., Jr.; and Witte, William G.: Flight-Test Analysis of Apollo Heat-Shield Material Using the Pacemaker Vehicle System. NASA TN D-4713, 1968.

12. LeBel, Peter J.; and Russell, James M., III: Development of Sensors To Obtain In-Flight Ablation Measurements of Thermal-Protection Materials. NASA TN D-3686, 1966.

13. Stroud, C. W.: A study of the Reaction-Plane Approximation in Ablation Analyses. NASA TN D-4817, 1968.

14. Wells, P. B.: A Method for Predicting the Thermal Response of Charring Ablation Materials. Doc. No. D2-23256, Boeing Co., 1964.

15. Nydick, Sander E.: Thermocouple Errors in Ablation Materials. Preprint No. 16.12-3-66, Instrum. Soc. Amer., Oct. 1966.

16. Brewer, William D.: Effect of Thermocouple Wire Size and Configuration on Internal Temperature Measurements in a Charring Ablator. NASA TN D-3812, 1967.

17. Dow, Marvin B.: Comparison of Measurements of Internal Temperatures in Ablation Material by Various Thermocouple Configurations. NASA TN D-2165, 1964.

18. Exton, Reginald J.: Application of Photographic Pyrometry to Ablation Models. AIAA J., vol. 7, no. 12, Dec. 1969, pp. 2262-2266.

19. Wakefield, Roy M.; and Lundell, John H.: Comparison of the Performance of a Charring Ablator Under Transient and Constant Combined Convective and Radiative Heating. AIAA Paper No. 69-151, Jan. 1969.

20. Wilson, R. Gale, compiler: Thermophysical Properties of Six Charring Ablators From 140° to 700° K and Two Chars From 800° to 3000° K. NASA TN D-2991, 1965.

21. Farmer, Rex W.: Thermogravimetry of Plastics. Pt. I: Empirical Homogeneous Kinetics. ASD-TDR-62-1043, Pt. I, U.S. Air Force, Feb. 1963.

22. Wilson, R. Gale: Hemispherical Spectral Emittance of Ablation Chars, Carbon, and Zirconia to 3700° K. NASA TN D-2704, 1965.

TABLE I.- LOCATION OF INSTRUMENTATION

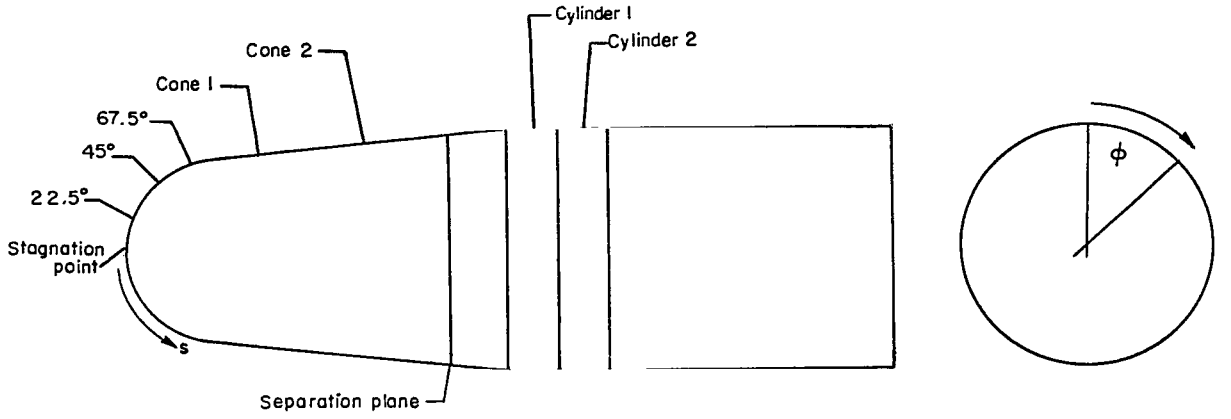

Circumferential location, ø (a)	Spacecraft station	Surface distance, cm (in.)	Dual Ablation sensor	Spring-wire sensor	3-element thermocouple plugs
0°	Stagnation point	0	Yes		
	22.5°	3.81 (1.5)		Yes	
	45°	7.62 (3.0)			Yes
	67.5°	11.43 (4.5)	Yes		
60°	67.5°	11.43 (4.5)		Yes	
70°	Cylinder 1	45.0 (17.72)	Yes		
120°	45°	7.62 (3.0)		Yes	
	67.5°	11.43 (4.5)		Yes	
180	22.5°	3.81 (1.5)	Yes		
	67.5°	11.43 (4.5)		Yes	
	Cone 1	18.24 (7.18)			Yes
210°	Cone 2	28.43 (11.20)			Yes
240°	45°	7.62 (3.0)		Yes	
250°	Cylinder 2	50.1 (19.72)	Yes		
300°	45°	7.62 (3.0)	Yes		
315°	Cylinder 1	45.0 (17.72)			Yes

[a]Circumferential locations are measured clockwise, looking at the spacecraft from the front.

TABLE II.- ABLATION DATA

(a) Spring-wire ablation rate sensor data

Spacecraft station	Circumferential location, ϕ	Sensing depth, cm (in.) (a)	Time triggered, sec (b)		
			Event-recorder data		Telemetered data
			Earliest	Latest	
Stagnation point	0°	0.089 (0.035)	76.27	76.29	76.28
		.152 (.060)	82.97	82.98	83.06
		.406 (.160) P	N.T.	N.T.	N.T.
		.787 (.310) P	N.T.	N.T.	N.T.
22.5°	180°	0.064 (0.025) (thru)	74.01	74.02	74.00
		.330 (.130)	106.81	106.84	106.81
		.787 (.310) P	N.T.	N.T.	N.T.
		.978 (.385)	N.T.	N.T.	N.T.
22.5°	0°	0.066 (0.026) (thru)	73.57	73.58	73.61
		.114 (.045)	76.94	77.03	Not TM
		.216 (.085)	84.04	84.07	84.17
		.658 (.259) P	N.T.	N.T.	N.T.
45°	120°	0.117 (0.046)	74.63	74.64	Not TM
		.368 (.145)	82.82	82.83	Not TM
		1.549 (.610)	N.T.	N.T.	Not TM
		1.930 (.760)	N.T.	N.T.	N.T.
45°	240°	0.076 (0.030)	74.75	74.76	74.79
		.218 (.086)	76.09	76.11	76.15
		.470 (.185) (thru)	87.82	87.84	88.01
		1.143 (.450)	N.T.	N.T.	N.T.
45°	300°	0.089 (0.035) (thru)	73.37	73.43	73.89
		.142 (.056)	74.71	74.72	74.77
		.279 (.110)	79.40	79.45	79.49
		.737 (.290)	123.96	124.05	123.82
67.5°	0°	0.061 (0.024)	80.96	80.98	80.95
		.112 (.044)	81.42	81.45	81.54
		.213 (.084)	Not Rec	Not Rec	82.04
		.660 (.260) P	N.T.	N.T.	Not TM
67.5°	120°	0.076 (0.030)	83.39	83.41	83.52
		.102 (.040)	85.12	85.16	85.22
		.279 (.110)	102.26	102.33	Not TM
		.901 (.355)	Not Rec	Not Rec	N.T.
67.5°	60°	0.102 (0.040)	83.03	83.10	83.18
		.406 (.160)	100.94	100.98	101.02
		1.169 (.460)	N.T.	N.T.	Not TM
		1.298 (.511)	Not Rec	Not Rec	N.T.
67.5°	180°	0.064 (0.025) (thru)	81.37	81.39	81.50
		.127 (.050)	90.13	90.20	90.18
		.533 (.209)	128.18	128.22	Not TM
		.787 (.310)	Not Rec	Not Rec	N.T.

[a] P indicates that during the flight test the sensor tube became exposed above the heat-shield surface but was not triggered; (thru) indicates that the spring-wire sensor was located at its effective sensing depth in a hole drilled completely through the heat-shield material.

[b] N.T. indicates that the spring-wire sensor was unaffected by flight (i.e., not triggered); Not TM indicates that data signals applied to event recorder only (i.e., not telemetered); and Not Rec indicates that data signals applied to telemeter only (i.e., not recorded).

TABLE II.- ABLATION DATA – Concluded

(b) Make-wire ablation rate sensor data

Spacecraft station	Circumferential location, ϕ	Sensing depth, cm (in.)	Time triggered, sec (a)
Stagnation point	0°	0.038 (0.015)	71.80
		.102 (.040)	73.41
		.356 (.140)	88.24
		.737 (.290)	136.45
22.5°	180°	0.013 (0.005)	71.75
		.279 (.110)	84.59
		.737 (.290)	132.87
		.927 (.365)	N.T.
45°	300°	0.025 (0.010)	72.09
		.091 (.036)	73.37
		.229 (.090)	76.37
		.686 (.270)	92.79
67.5°	0°	0.010 (0.004)	72.85
		.061 (.024)	75.52
		.163 (.064)	81.33
		.610 (.240)	118.62
Cylinder 1	70°	0.000 (0.000)	N.T.
		.064 (.025)	N.T.
		.127 (.050)	N.T.
		.229 (.090)	N.T.
Cylinder 2	250°	0.000 (0.000)	N.T.
		.064 (.025)	N.T.
		.127 (.050)	N.T.
		.229 (.090)	N.T.

[a] N.T. denotes that the make-wire sensor was unaffected by flight (i.e., not triggered).

TABLE III.- THERMOCOUPLE DEPTHS

[3-element thermocouples]

Spacecraft station	Initial sensing depth of –		
	Element 1	Element 2	Element 3
45°	Surface	0.244 cm (0.096 in.)	0.493 cm (0.194 in.)
Cone 1	Surface	.244 cm (.096 in.)	.500 cm (.197 in.)
Cone 2	Surface	.229 cm (.090 in.)	.500 cm (.197 in.)
Cylinder 1	Surface	.251 cm (.099 in.)	.510 cm (.201 in.)

TABLE IV.- SUMMARY OF POSTFLIGHT MEASUREMENTS

Station	Initial ablator thickness, mm (in.)	Average total surface recession, mm (in.)	Char and pyrolysis-zone thickness, mm (in.)
Stagnation point	24.4 (0.96)	8.64 (0.34)	0.51 (0.02)
22.5°	24.4 (0.96)	8.64 (0.34)	.76 (0.03)
45°	24.4 (0.96)	10.67 (0.42)	.76 (0.03)
67.5°	24.4 (0.96)	8.89 (0.35)	1.02 (0.04)
Cone 1	20.3 (0.8)	0.25 (0.01) estimated	1.27 (0.05)
Cone 2	14.2 (0.56)	0.25 (0.01) estimated	1.27 (0.05)
Cylinder 1	15.2 (0.6)	----------	.76 (0.03)

TABLE V.- MATERIAL PROPERTIES

(a) Virgin material

Density	1201 kg/m^3	(75 lbm/ft^3)
	kJ/kg-^{o}K	(Btu/lbm-^{o}R)
Specific heat (ref. 20):		
At 256^o K (460^o R)	1.28	(0.3)
At 311^o K (560^o R)	1.54	(0.362)
At 367^o K (660^o R)	1.79	(0.421)
At 422^o K (760^o R)	2.04	(0.48)
At 478^o K (860^o R)	2.28	(0.536)
At 533^o K (960^o R)	2.53	(0.595)
At 589^o K (1060^o R)	2.79	(0.657)
At 700^o K (1260^o R)	3.27	(0.769)
	W/m-^{o}K	(Btu/ft-sec-^{o}R)
Thermal conductivity (ref. 20):		
At 256^o K (460^o R)	0.337	(5.19×10^{-5})
At 311^o K (560^o R)	0.356	(5.48×10^{-5})
At 367^o K (660^o R)	0.367	(5.64×10^{-5})
At 422^o K (760^o R)	0.369	(5.68×10^{-5})
At 478^o K (860^o R)	0.364	(5.60×10^{-5})
At 533^o K (960^o R)	0.348	(5.36×10^{-5})
At 589^o K (1060^o R)	0.325	(5.00×10^{-5})
At 2779^o K (5000^o R)	0.325	(5.00×10^{-5})
Pyrolysis reaction constants (ref. 21):		
Frequency factor	17.2 Gg/m^3-sec	(1.07×10^6 lb/ft^3-sec)
Activation energy	98 kJ/mole	(2.34×10^4 cal/mole)
Order of equation	1	
Heat of pyrolysis	11.6 MJ/kg	(500 Btu/lbm)

TABLE V.- MATERIAL PROPERTIES – Concluded

(b) Charred material

	kg/m^3	(lbm/ft^3)
Density (ref. 1):		
Stagnation point	480	(30)
22.5^o station	480	(30)
45^o station	400	(25)
67.5^o station	400	(25)
Cone	384	(24)
Cylinder	368	(23)

	Of char		Of pyrolysis gas	
	kJ/kg-^{o}K	(Btu/lbm-^{o}R)	kJ/kg-^{o}K	(Btu/lbm-^{o}R)
Specific heat (ref. 20):				
At 400^o K (720^o R)	0.47	(0.11)	1.70	(0.4)
At 600^o K (1080^o R)	1.02	(0.24)	2.76	(0.65)
At 700^o K (1260^o R)	1.28	(0.30)	3.91	(0.92)
At 800^o K (1440^o R)	1.49	(0.35)	6.16	(1.45)
At 900^o K (1620^o R)	1.74	(0.41)	10.41	(2.45)
At 1000^o K (1800^o R)	2.00	(0.47)	12.11	(2.85)
At 1200^o K (2160^o R)	2.51	(0.59)	8.29	(1.95)
At 1400^o K (2520^o R)	2.76	(0.65)	5.10	(1.20)
At 1500^o K (2700^o R)	2.85	(0.67)	4.04	(0.95)
At 1600^o K (2880^o R)	2.85	(0.67)	3.70	(0.87)
At 1800^o K (3240^o R)	2.85	(0.67)	3.44	(0.81)
At 2000^o K (3600^o R)	2.85	(0.67)	3.53	(0.83)
At 2200^o K (3960^o R)	2.85	(0.67)	3.82	(0.90)
At 2400^o K (4320^o R)	2.85	(0.67)	4.46	(1.05)
At 2600^o K (4680^o R)	2.85	(0.67)	5.40	(1.27)
At 2800^o K (5040^o R)	2.85	(0.67)	6.59	(1.55)
At 3000^o K (5400^o R)	2.85	(0.67)	8.29	(1.95)

	W/m-^{o}K	(Btu/ft-sec-^{o}R)
Thermal conductivity (ref. 20):		
At 533^o K (960^o R)	0.100	(1.55×10^{-4})
At 811^o K (1460^o R)	0.103	(1.58×10^{-4})
At 1089^o K (1960^o R)	0.114	(1.75×10^{-4})
At 1367^o K (2460^o R)	0.131	(2.02×10^{-4})
At 1645^o K (2960^o R)	0.157	(2.42×10^{-4})
At 1922^o K (3460^o R)	0.193	(2.97×10^{-4})
At 2200^o K (3960^o R)	0.244	(3.75×10^{-4})
At 2479^o K (4460^o R)	0.311	(4.78×10^{-4})
At 2755^o K (4960^o R)	0.423	(6.50×10^{-4})
At 3033^o K (5460^o R)	0.542	(8.34×10^{-4})

Emissivity (ref. 22) 0.95

Heat of combustion . . . . . 116 MJ/kg (5000 Btu/lbm)

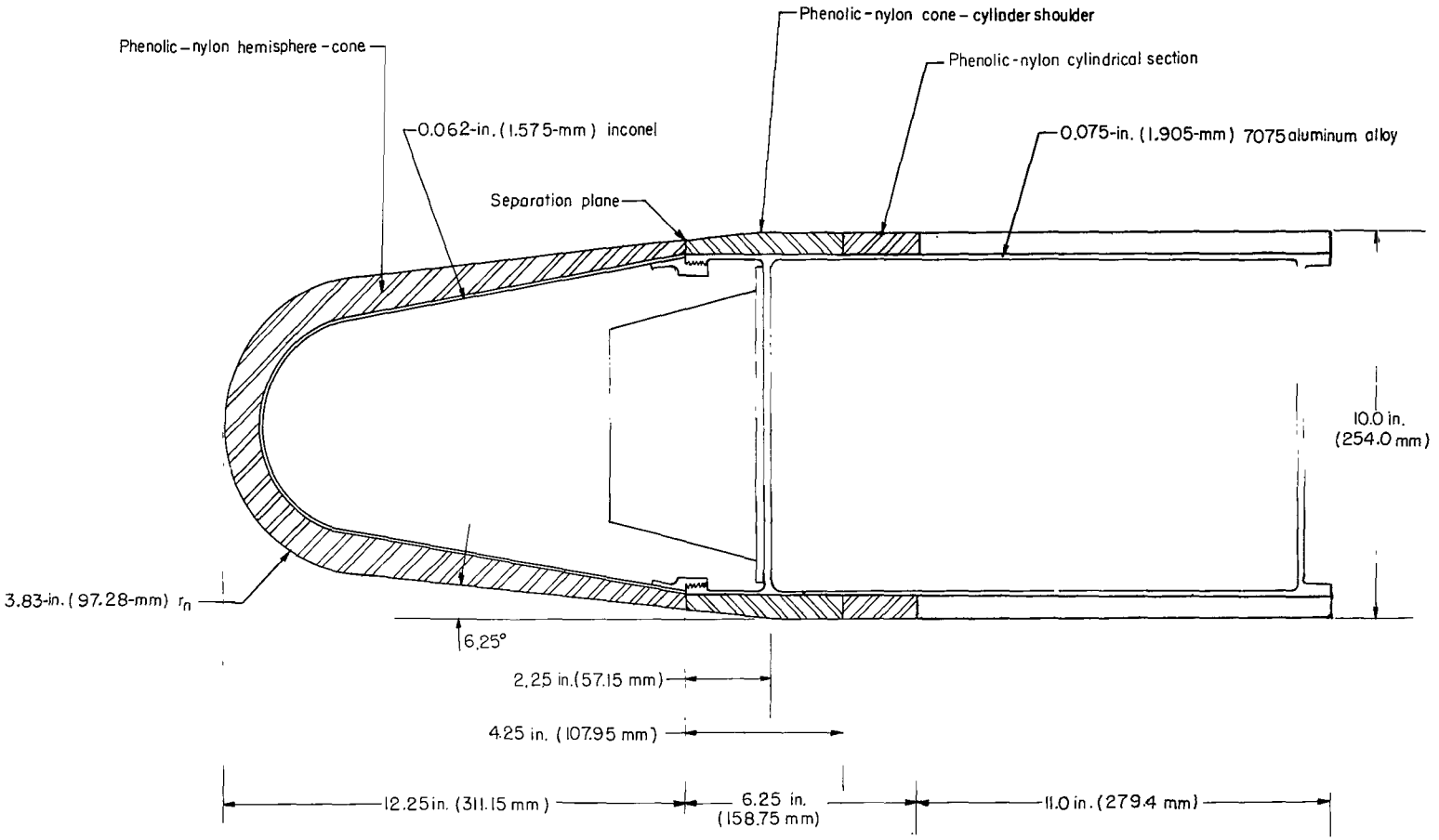

Figure 1.- Sketch of the spacecraft.

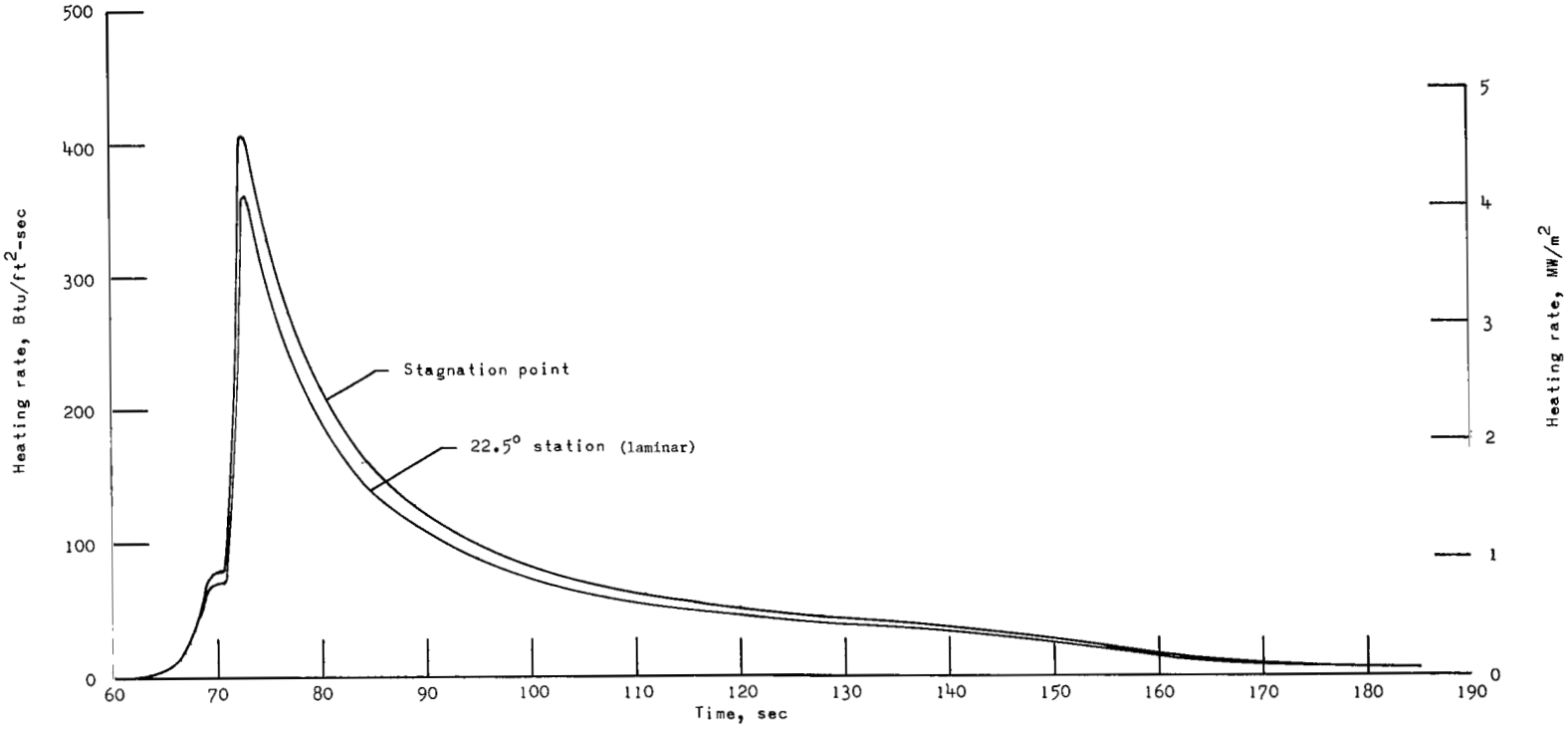

(a) Stagnation point and 22.5° station.

Figure 2.- Computed cold-wall heating rates.

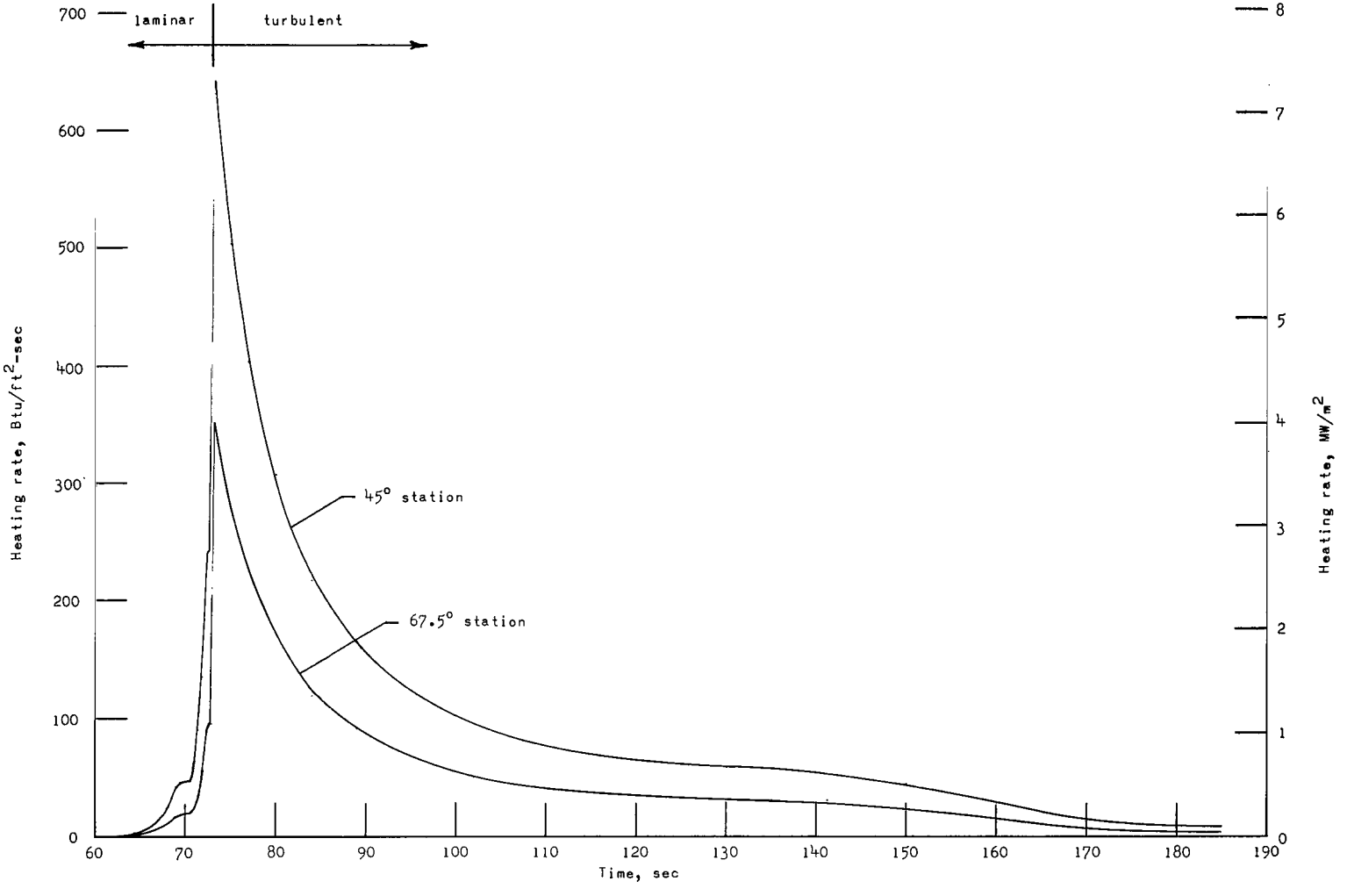

(b) 45° station and 67.5° station.

Figure 2.- Continued.

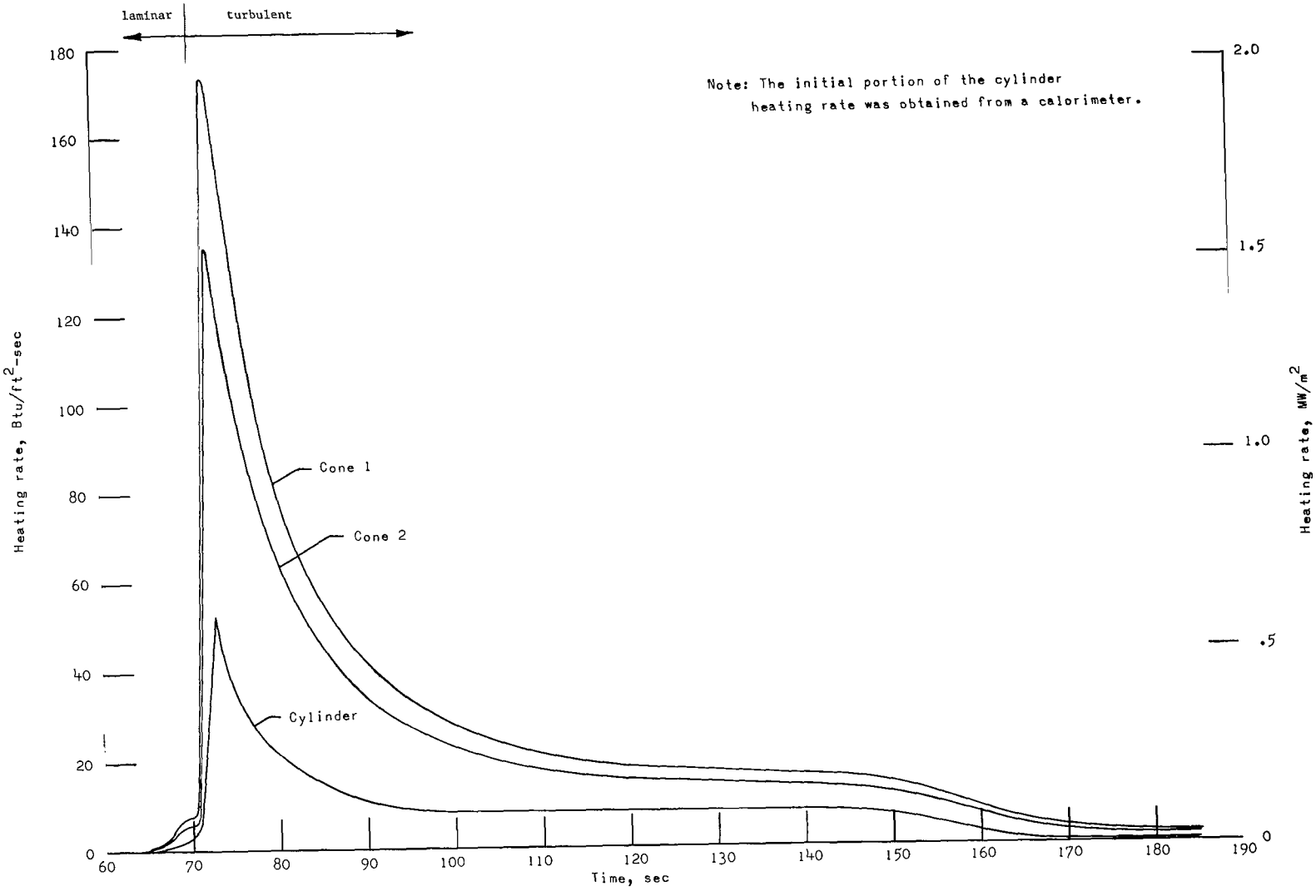

(c) Cone and cylinder.

Figure 2.- Concluded.

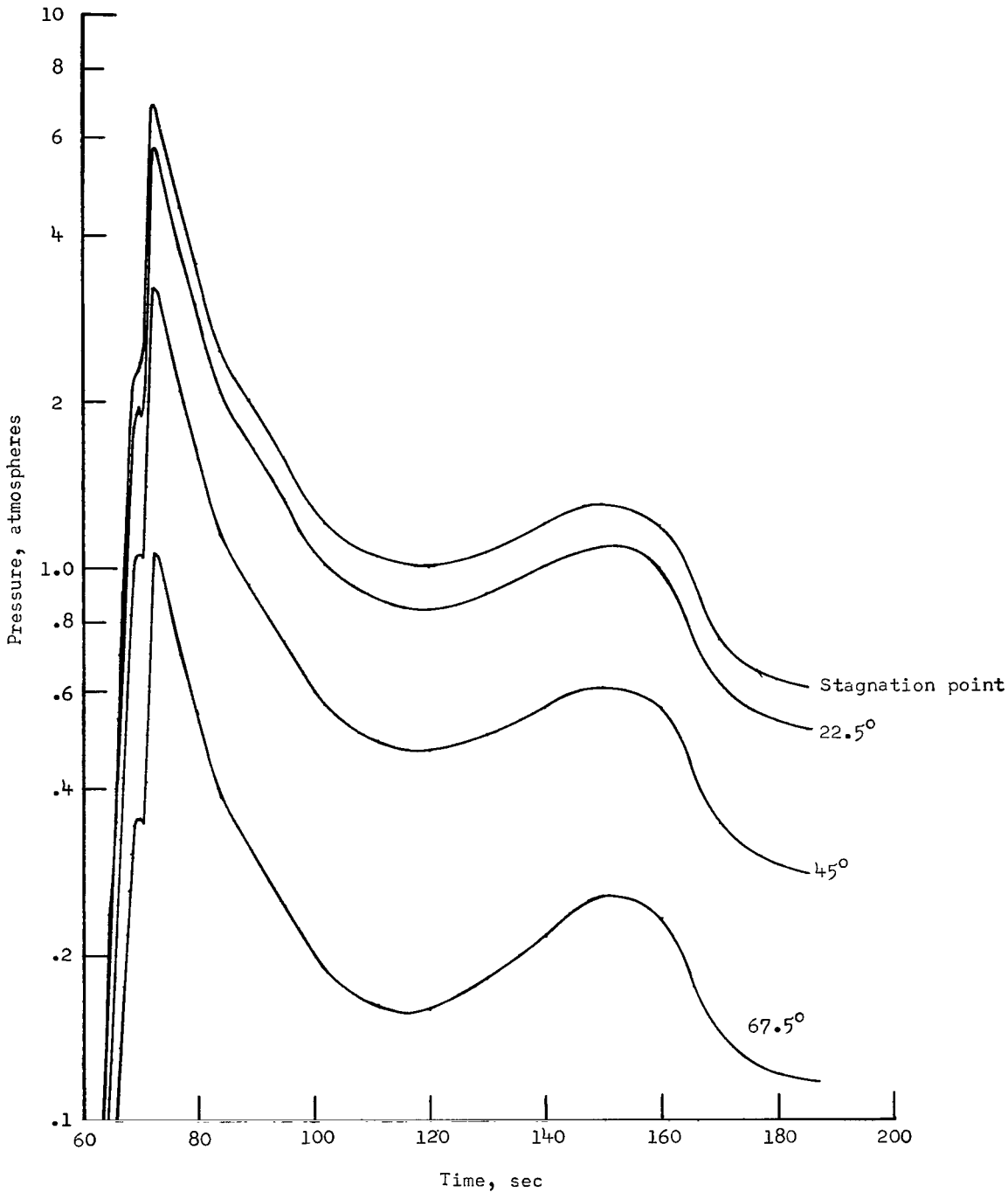

(a) Stations on the hemisphere.

Figure 3.- Computed time histories of local pressures.

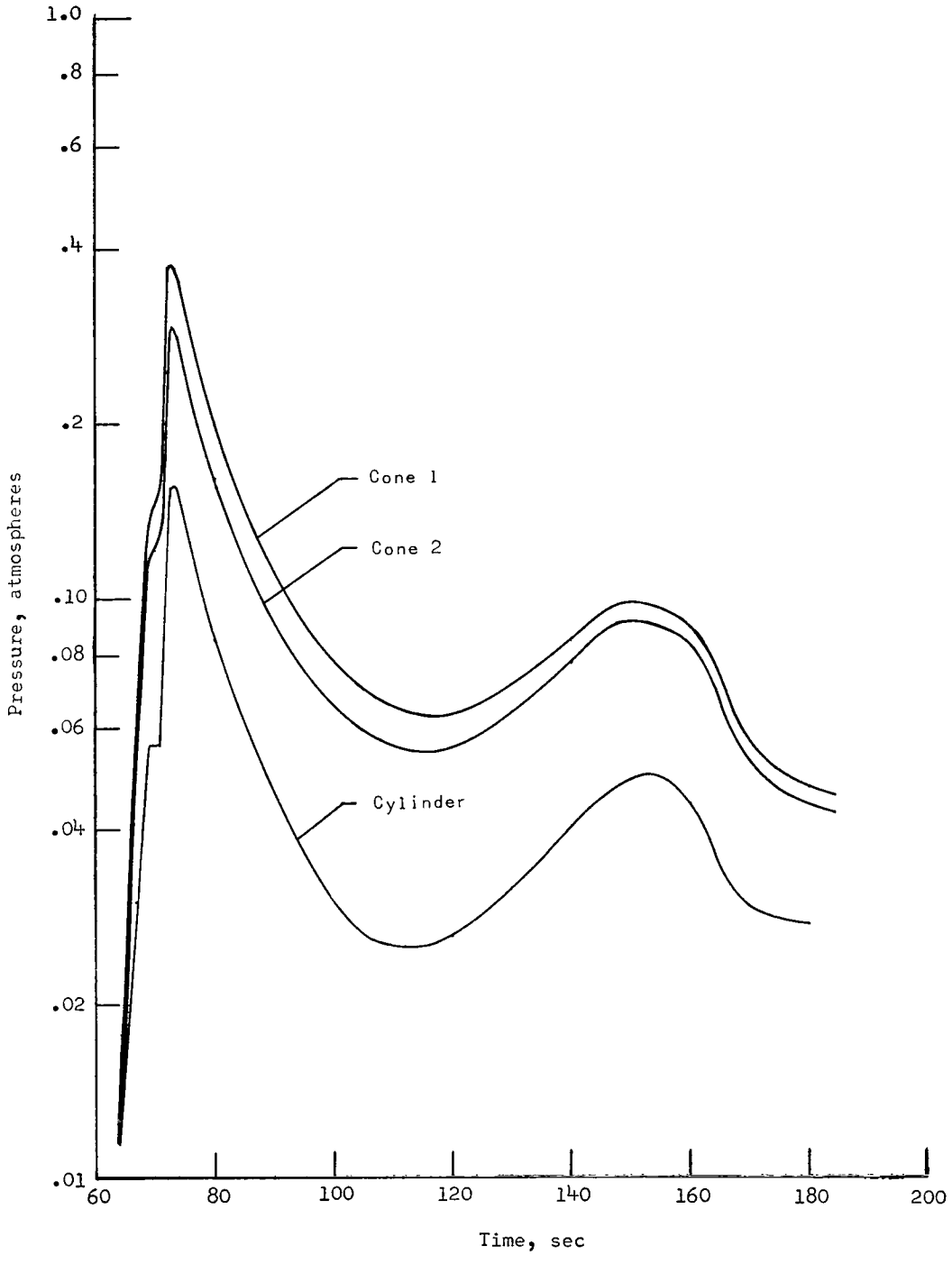

(b) Stations on the cone and cylinder.

Figure 3.- Concluded.

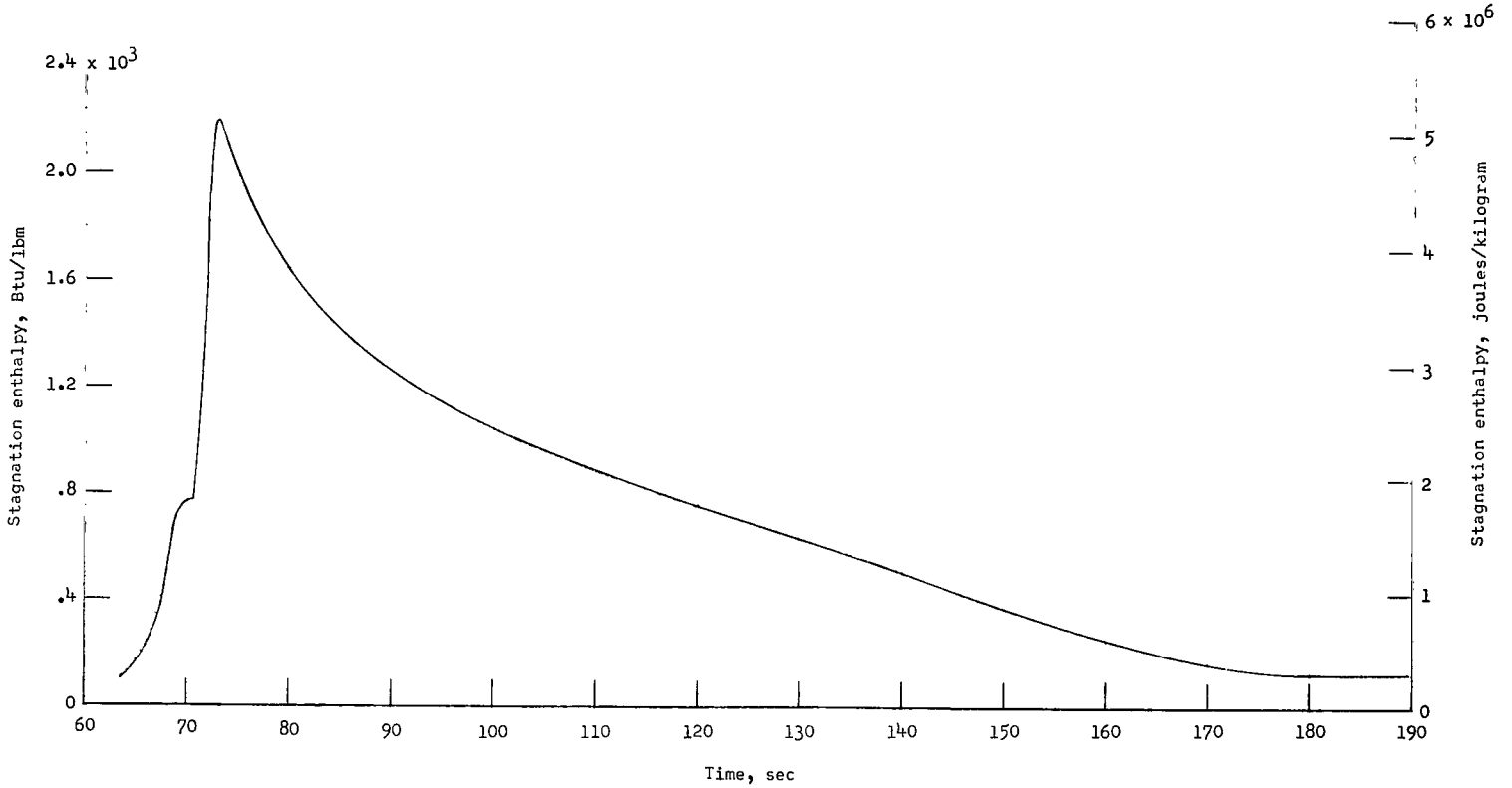

Figure 4.- Computed time history of stagnation enthalpy.

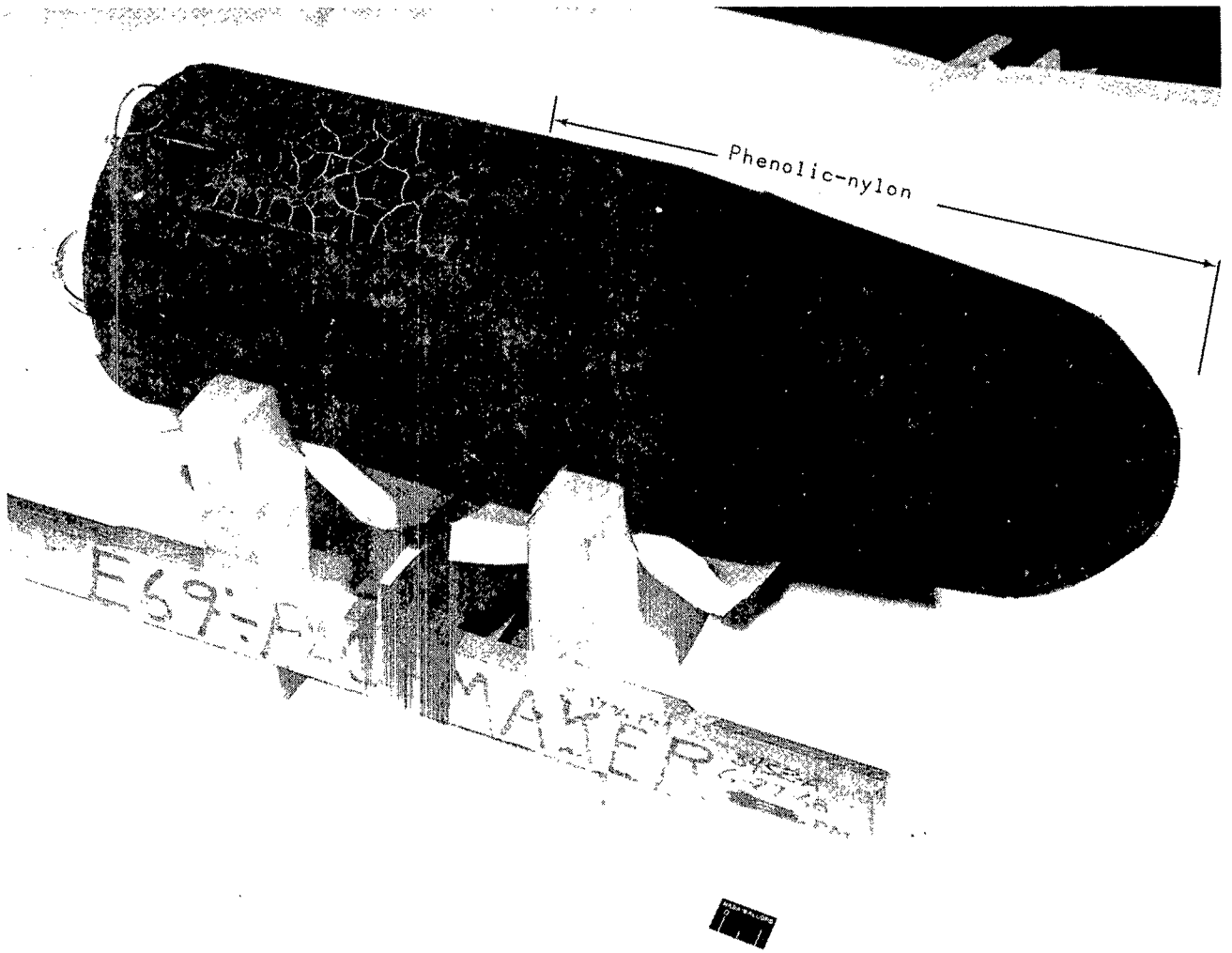

L-68-4515.1

Figure 5.- Photograph of the recovered spacecraft.

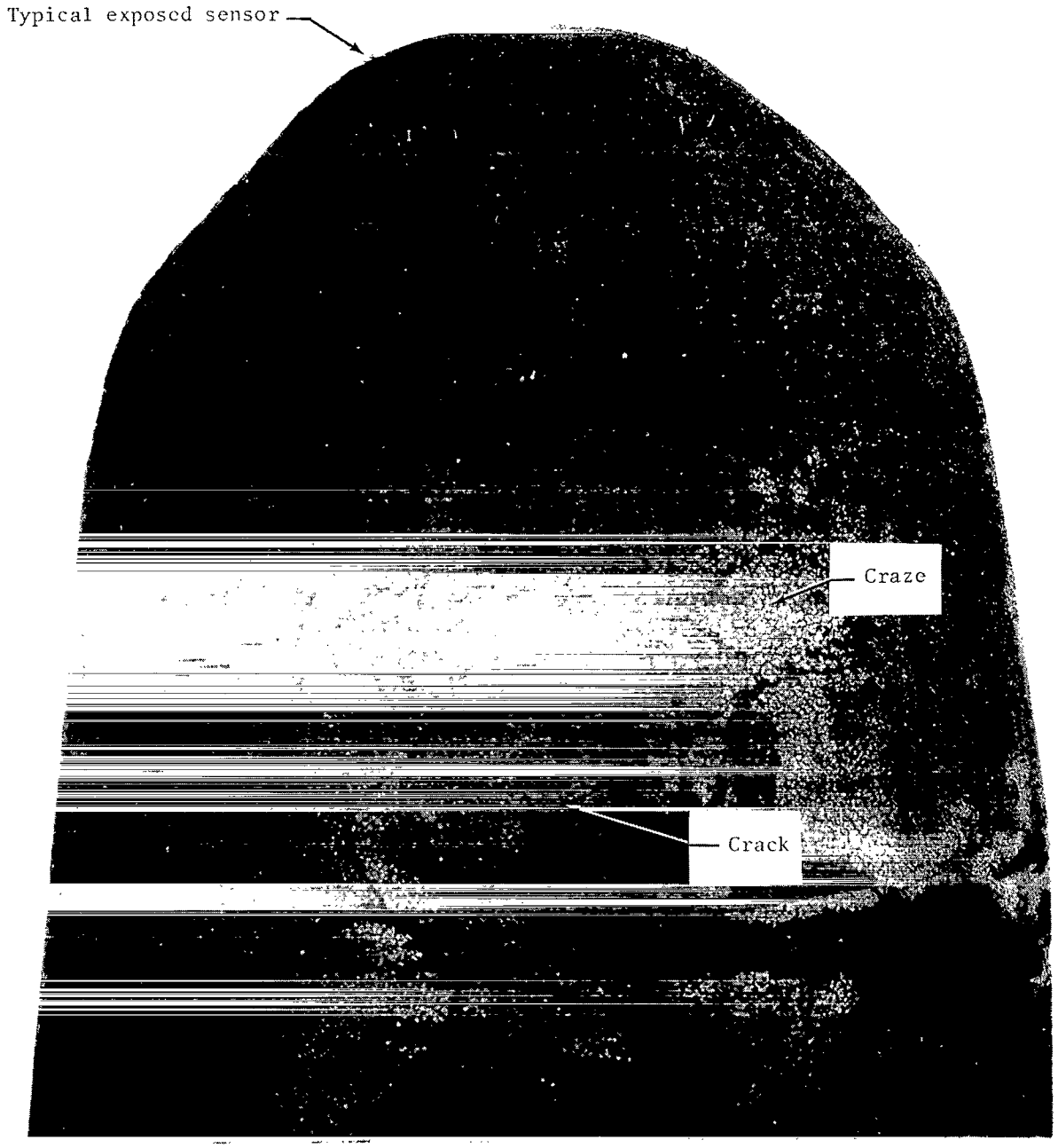

L-69-5390.2

Figure 6.- Close-up of the hemisphere.

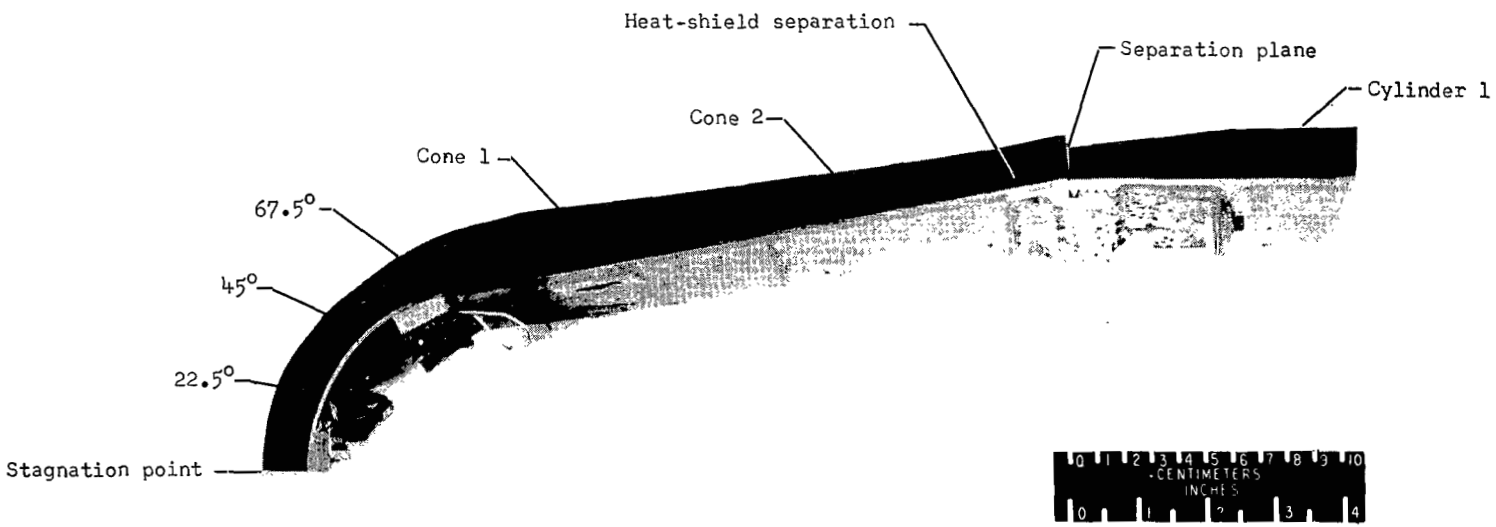

L-69-4728.2

Figure 7.- Section of phenolic-nylon taken from the recovered spacecraft, showing the 60° circumferential location.

L-68-5785.1

Figure 8.- Close-up of the cone-cylinder juncture and cylinder.

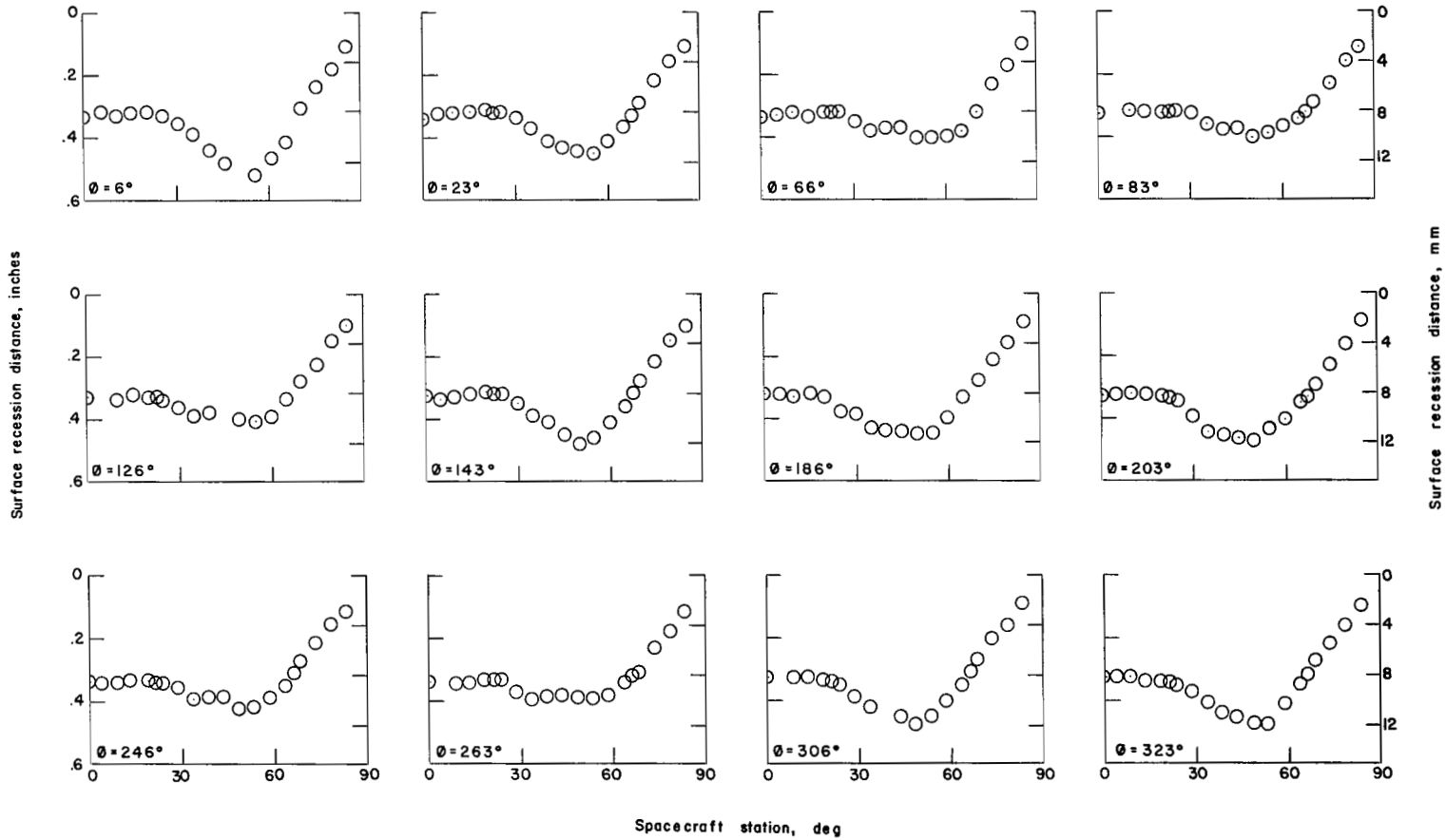

Figure 9.- Postflight measurements of the profile change on the hemisphere.

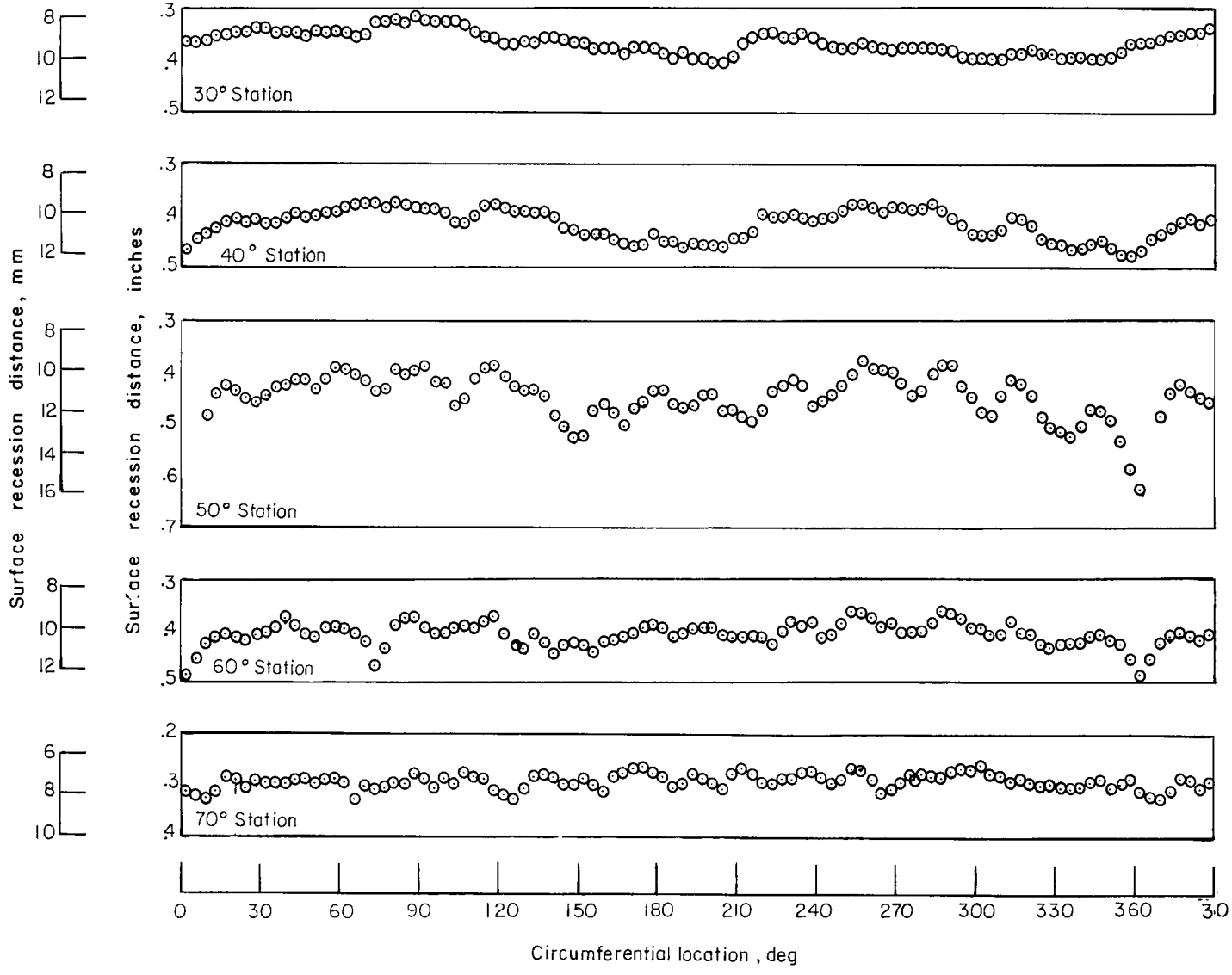

Figure 10.- Circumferential profile change measurements at the 30°, 40°, 50°, 60°, and 70° stations on the hemisphere.

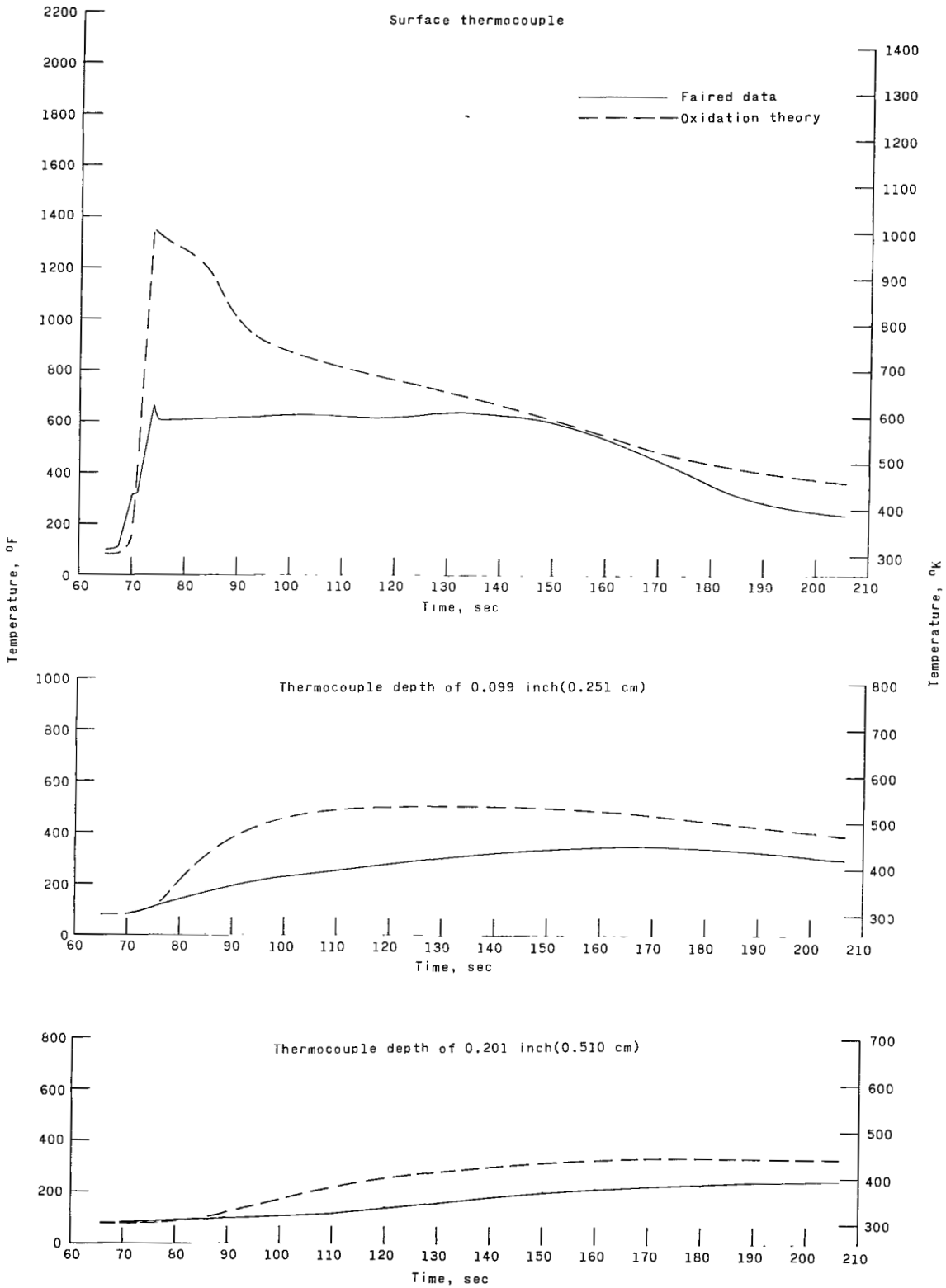

(c) Cylinder station 1.

Figure 11.- Concluded.

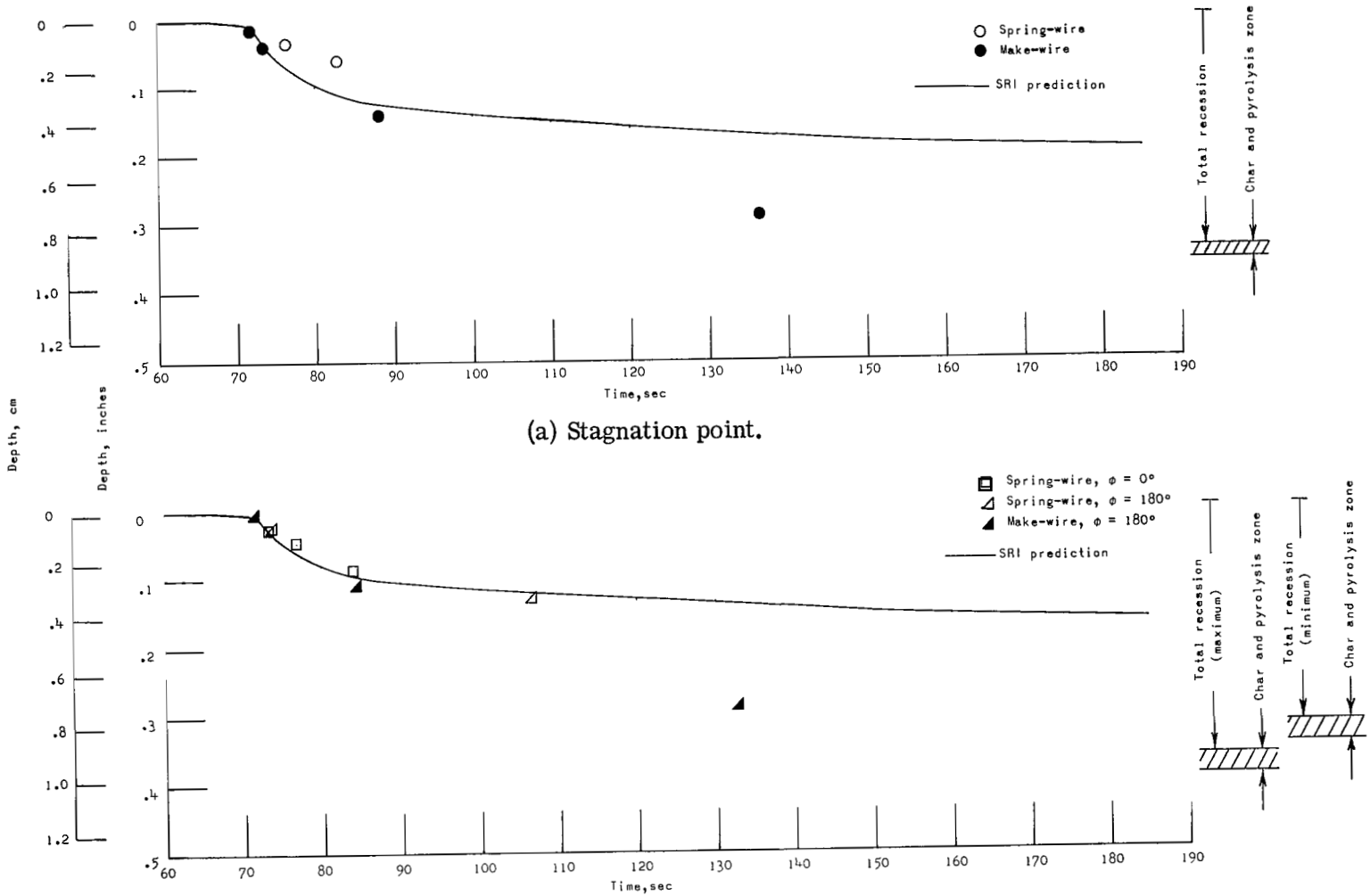

(a) Stagnation point.

(b) 22.5° station.

Figure 12.- Sensor data and postflight measurements at the stagnation point and at the 22.5° station compared with surface-recession predictions based on the SRI correlation.

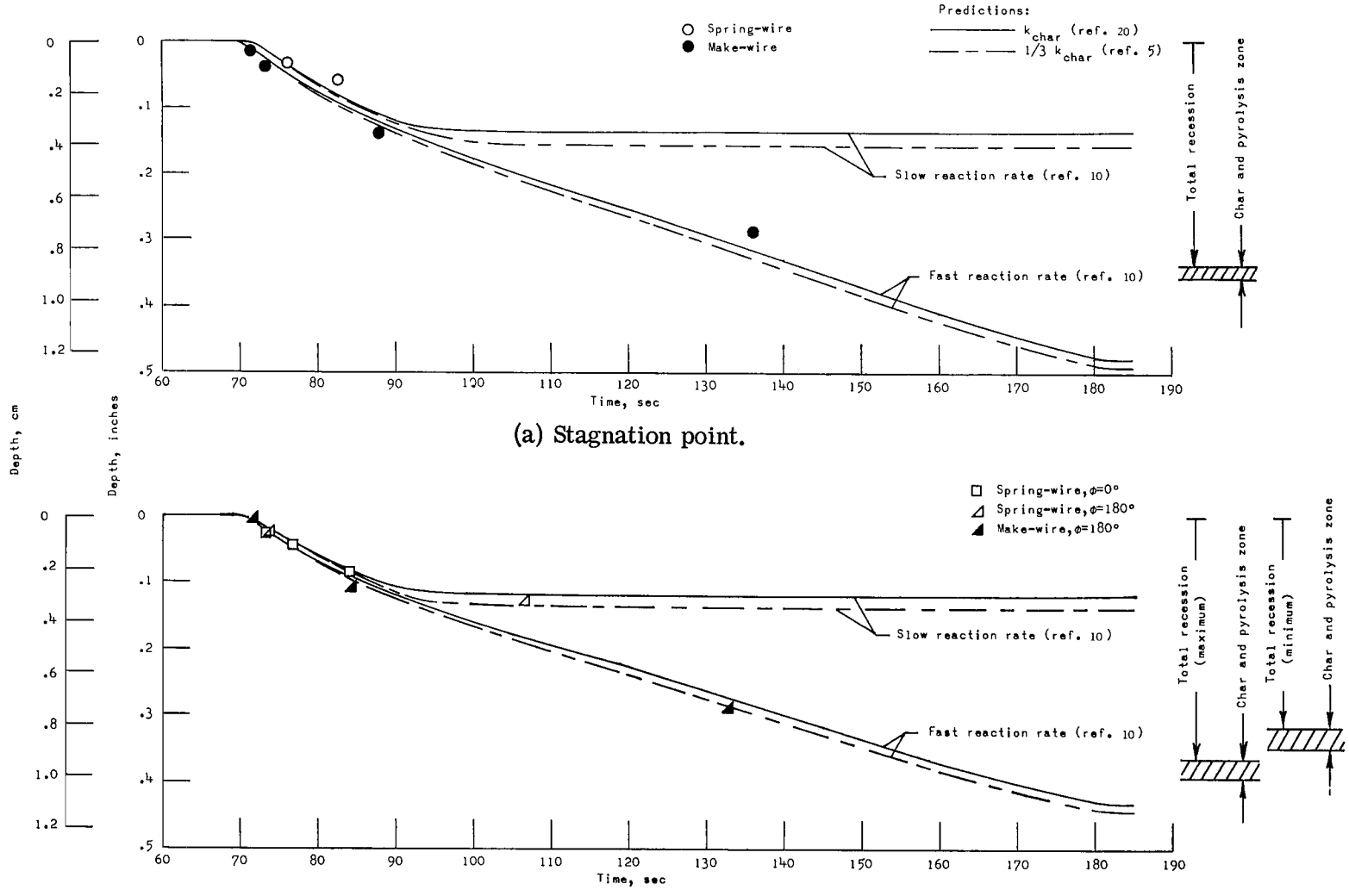

Figure 13.- Sensor data and postflight measurements on the hemisphere compared with surface-recession predictions calculated with oxidation theory.

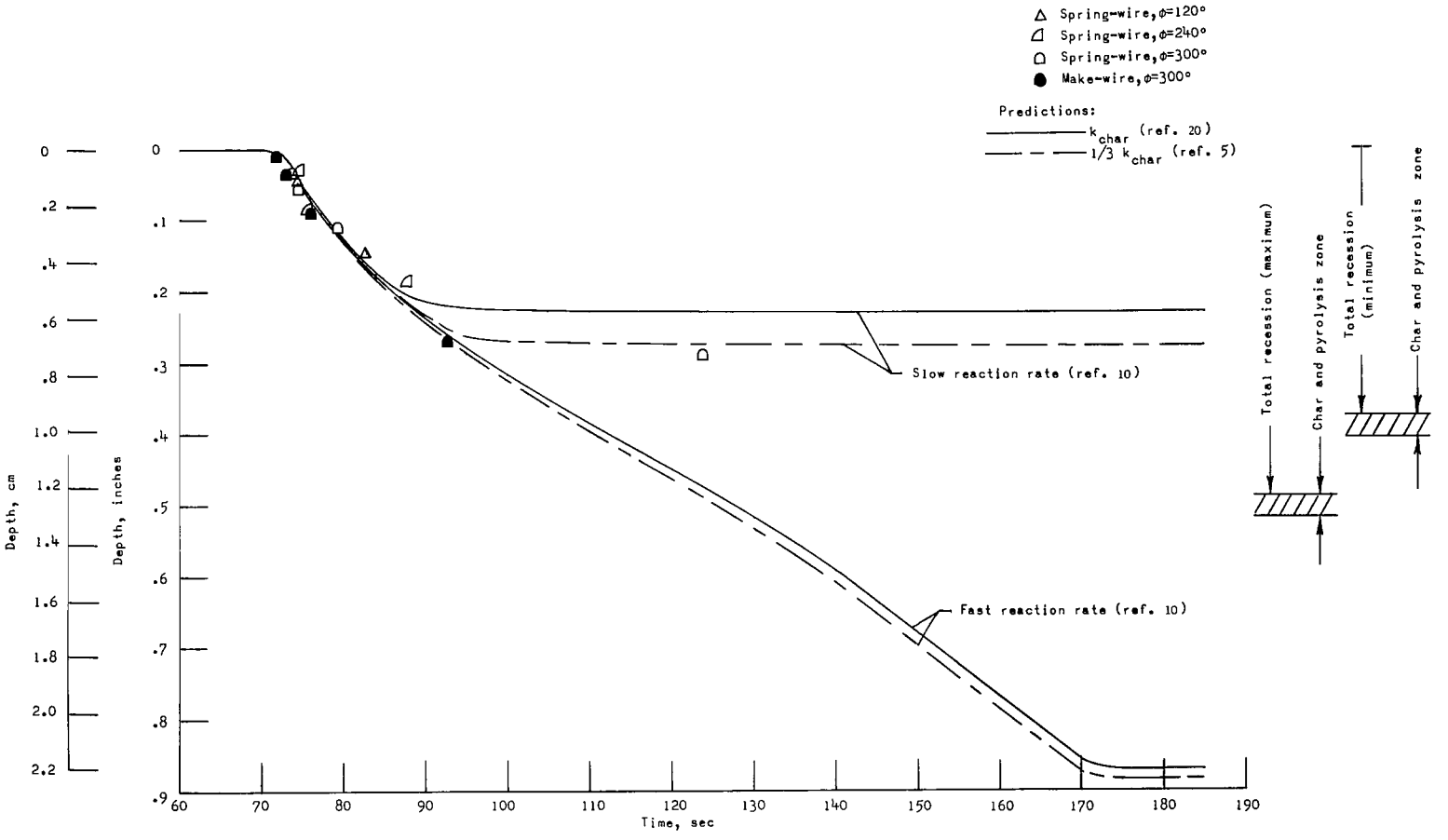

(c) 45° station.

Figure 13.- Continued.

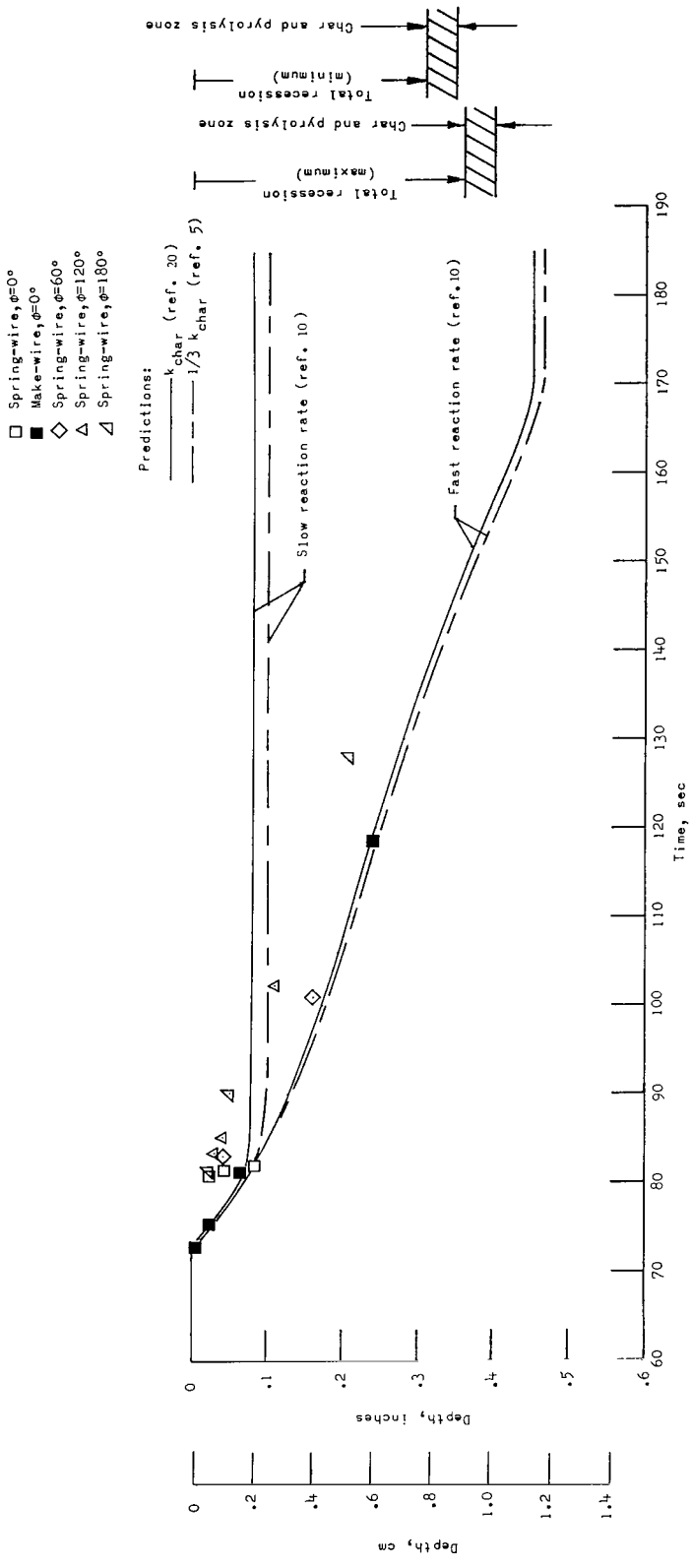

(d) 67.5^{o} station.

Figure 13.- Concluded.

NASA-Langley, 1971 —— 33 L-7230

08U 001 58 51 3DS 71135 00903
AIR FORCE WEAPONS LABORATORY /WLOL/
KIRTLAND AFB, NEW MEXICO 87117

ATT E. LOU BOWMAN, CHIEF,TECH. LIBRARY

"The aeronautical and space activities of the United States shall be conducted so as to contribute . . . to the expansion of human knowledge of phenomena in the atmosphere and space. The Administration shall provide for the widest practicable and appropriate dissemination of information concerning its activities and the results thereof."

—NATIONAL AERONAUTICS AND SPACE ACT OF 1958

NASA SCIENTIFIC AND TECHNICAL PUBLICATIONS

TECHNICAL REPORTS: Scientific and technical information considered important, complete, and a lasting contribution to existing knowledge.

TECHNICAL NOTES: Information less broad in scope but nevertheless of importance as a contribution to existing knowledge.

TECHNICAL MEMORANDUMS: Information receiving limited distribution because of preliminary data, security classification, or other reasons.

CONTRACTOR REPORTS: Scientific and technical information generated under a NASA contract or grant and considered an important contribution to existing knowledge.

TECHNICAL TRANSLATIONS: Information published in a foreign language considered to merit NASA distribution in English.

SPECIAL PUBLICATIONS: Information derived from or of value to NASA activities. Publications include conference proceedings, monographs, data compilations, handbooks, sourcebooks, and special bibliographies.

TECHNOLOGY UTILIZATION PUBLICATIONS: Information on technology used by NASA that may be of particular interest in commercial and other non-aerospace applications. Publications include Tech Briefs, Technology Utilization Reports and Technology Surveys.

Details on the availability of these publications may be obtained from:

SCIENTIFIC AND TECHNICAL INFORMATION OFFICE

NATIONAL AERONAUTICS AND SPACE ADMINISTRATION

Washington, D.C. 20546